



Eustasy in the Aptian world: A vision from the eastern margin of the Iberian Plate

Telm Bover-Arnal^{a,b,*}, Ramon Salas^{a,b}, Joan Guimerà^{b,c}, Josep Anton Moreno-Bedmar^d

^a Departament de Mineralogia, Petrologia i Geologia Aplicada, Facultat de Ciències de la Terra, Universitat de Barcelona, Martí i Franquès s/n, 08028 Barcelona, Catalonia, Spain

^b Institut de Recerca UB-GEOMODELS, c/ Martí Franquès s/n, 08028 Barcelona, Catalonia, Spain

^c Departament de Dinàmica de la Terra i de l'Oceà, Facultat de Ciències de la Terra, Universitat de Barcelona, Martí i Franquès s/n, 08028 Barcelona, Catalonia, Spain

^d Instituto de Geología, Universidad Nacional Autónoma de México, Ciudad Universitaria, Coyoacán, 04510 Ciudad de México, Mexico

ARTICLE INFO

Editor: Alan Haywood

Keywords:

Sea-level changes
Amplitude of sea-level changes
Cretaceous eustasy
Carbonate platform
Incised valley
Sequence stratigraphy
Forced regression
Aptian
Maestrat Basin
Iberian Plate

ABSTRACT

Eustatic controls on Early Cretaceous (Aptian) sedimentation in the western Tethys are discerned in outcrops of carbonate platforms that developed in the Maestrat rift basin located at the eastern margin of the Iberian Plate. The relative sea-level fluctuations with a dominant eustatic contribution investigated had estimated magnitudes of between 50 and 60 m in <0.9 My and ≥ 115 m in <3 My, and occurred respectively during the late early and early late Aptian. The major relative sea-level falls of mainly eustatic nature were recorded as forced regressive sedimentary wedges or as incised valleys carved into highstand carbonate platforms, whereas the subsequent sea-level rises back-filled the incised topographic lows created, or favoured the development of lowstand platforms. The finding of 50–115 m amplitude fluctuations of Aptian age is of relevance in that show magnitudes of relative sea-level fall in the order of that recorded during the last glacial maximum in the late Pleistocene (c. 120 m). The current knowledge on Cretaceous climate history shows an Earth with non-uniform greenhouse conditions. However, geological evidence of temporary icehouse states with ice-cap magnitudes close to late Pleistocene scales during the Aptian is absent, or at least has not been reported so far. Thus, although falling within the glacio-eustatic domain, the driving processes of these widespread drops and subsequent rises in relative sea level remain a mystery. Finally, this paper is an example of how sequence stratigraphy can be applied to carbonate successions, and of how this methodology indeed permits to unravel ancient relative sea-level fluctuations which controlled carbonate production and accumulation.

1. Introduction

An open question of the Earth's past oceanographic dynamics is the nature of Cretaceous relative sea-level changes with amplitudes of tens of metres and durations varying between 0.5 and 3 My, which have been described in several basins from the geologic past (e.g., Miall, 1997; Strasser et al., 2000; Immenhauser, 2005; Boulila et al., 2011; Haq, 2014; Cloetingh and Haq, 2015; Hay, 2016). Although, intrinsic uncertainties of chronostratigraphic frameworks mainly based on chemo- and biostratigraphic data exist, comparatively contemporaneous sea-level changes of this magnitude and duration have been documented for different settings and tectonic plates (e.g., Cooper, 1977; Haq et al., 1987; Hardenbol et al., 1998; Röhl and Ogg, 1998; Miller et al., 2005;

Haq, 2014). Therefore, these third-order sea-level events (sensu Vail et al., 1991) are commonly interpreted as the result of eustatic forcings (e.g., Cooper, 1977; Vail et al., 1991; Boulila et al., 2011; Sames et al., 2016). The mechanisms contributing to eustatic sea-level fluctuations are ocean-atmosphere processes (dynamic changes), thermal expansion of water masses (thermosteric changes), tectono-eustasy, sedimento-eustasy, hydro-eustasy and glacio-eustasy (e.g., Rovere et al., 2016; Gronitz, 2017).

Early Cretaceous possible third-order sea-level fluctuations have been frequently, and tentatively linked to glacio-eustasy (e.g., Stoll and Schrag, 1996; Matthews and Frohlich, 2002; Gréselle and Pittet, 2005, 2010; Immenhauser, 2005; Bover-Arnal et al., 2009, 2014, 2015; van Buchem et al., 2010; Maurer et al., 2010, 2013; Raven et al., 2010;

* Corresponding author at: Departament de Mineralogia, Petrologia i Geologia Aplicada, Facultat de Ciències de la Terra, Universitat de Barcelona, Martí i Franquès s/n, 08028 Barcelona, Catalonia, Spain.

E-mail address: telm.boverarnal@ub.edu (T. Bover-Arnal).

<https://doi.org/10.1016/j.gloplacha.2022.103849>

Received 23 February 2022; Received in revised form 19 May 2022; Accepted 20 May 2022

Available online 24 May 2022

0921-8181/© 2022 The Authors. Published by Elsevier B.V. This is an open access article under the CC BY-NC-ND license (<http://creativecommons.org/licenses/by-nc-nd/4.0/>).

Husinec et al., 2012; Al-Husseini, 2013; Graziano and Raspini, 2015; Graziano et al., 2016; Zorina, 2016; Horner et al., 2019; Ray et al., 2019; Davies et al., 2020; Simmons et al., 2020). However, alternative mechanisms capable of triggering sea-level fluctuations of this order include regional- to plate-scale tectonic processes, interactions between mantle and lithosphere, formation of large igneous provinces, thermo-

eustasy, aquifer-eustasy, and variations in the volume of mid-oceanic ridges and sediment supply (e.g., Hay and Leslie, 1990; Cloetingh, 1991; Cronin, 1999; Immenhauser, 2005; Conrad, 2013; Haq, 2014; Cloetingh and Haq, 2015; Sames et al., 2016, 2020; Wendler and Wendler, 2016; Wendler et al., 2016; Li et al., 2018). Such potential factors could have also acted in combination or isolated giving rise to the

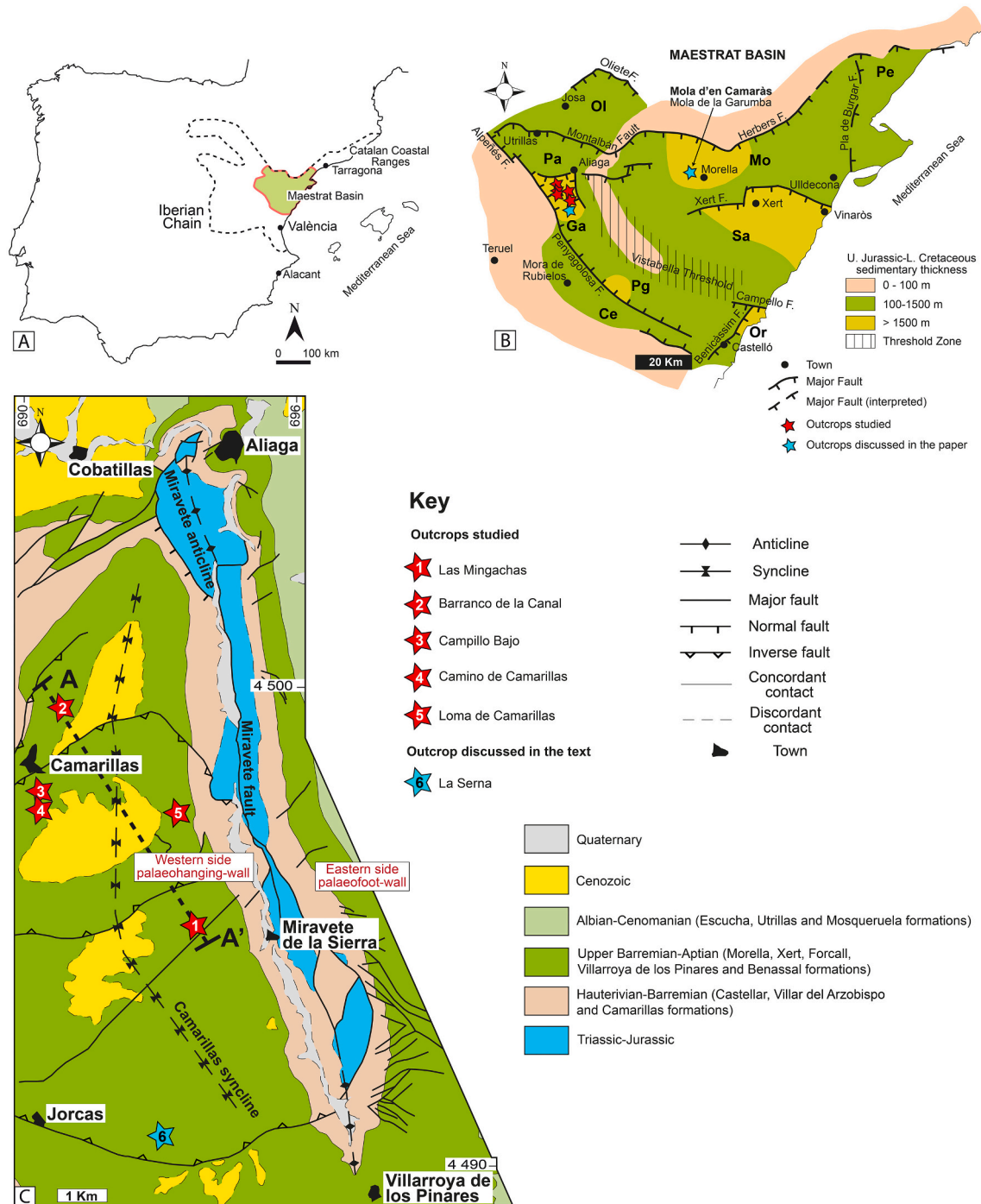


Fig. 1. A) Geographical location of the study area in the eastern Iberian Chain (E Iberia). B) Simplified isopach and structural map of the Maestrat Basin during the Late Jurassic and Early Cretaceous rifting cycles and location of the study localities in the Galve Sub-basin. The location of outcrops discussed in the paper are also indicated. Mo: Morella Sub-basin, Pe: El Perelló Sub-basin, Sa: La Salzedella Sub-basin, Ga: Galve Sub-basin, Ol: Oliete Sub-basin, Pa: Las Parras Sub-basin, Ce: Cedramán Sub-basin, Or: Orpesa Sub-basin, Pg: Penyagolosa Sub-basin. Modified after Salas et al. in [Martín-Chivelet et al. \(2019\)](#). The situation of the Campello Fault is taken from [Martín-Martín et al. \(2015\)](#). C) Geological map of the central Galve Sub-basin. The outcrops studied and discussed in the paper are respectively indicated with red and blue stars. Modified after [Canérot et al. \(1979\)](#) and [Gautier \(1980\)](#). The conceptual cross-section A-A' is shown in [Fig. 3C](#). Universal Transverse Mercator (UTM) Projection: Zone 30, Datum ETRS89. UTM coordinates are written in km. (For interpretation of the references to colour in this figure legend, the reader is referred to the web version of this article.)

third-order synchronous to parasynchronous sea-level events recognized in several Lower Cretaceous sedimentary basins.

In rift basins, local to regional tectonics is a key factor controlling accommodation. In such scenarios, it is of interest to discriminate and quantify the effects of eustasy from extensional tectonic factors (i.e., subsidence and uplift) in governing relative sea-level changes and thus, the sedimentary record. This paper presents two Early Cretaceous (Aptian) case studies from the Maestrat rift basin in the Iberian Chain that show sedimentary evidence of relative sea-level change mainly resulting from eustasy. The durations of the sea-level cycles interpreted from the Aptian record of the Maestrat Basin are of less than 3 My and show amplitudes of tens of metres, and therefore agree with third-order sea-level cycles (*sensu* Vail et al., 1991).

The investigations were carried out in the western marginal part of the basin. The marginal zone of a sedimentary basin, where accommodation is lower than in depocentral areas, is more likely to record unambiguous physical evidence (i.e., subaerial unconformities) of relative sea-level variations of distinct order. Accordingly, the Aptian successions studied exhibit erosional subaerial unconformities and/or forced regressive deposits resulting from major sea-level falls, as well as the sedimentary records of subsequent relative sea-level rises. The study aims to show that the eustatic or local to regional tectonic nature of past sea-level falls can be determined in the rock record based on the type of unconformity generated (disconformity *versus* angular unconformity). The paper also discusses the divergent interpretations (Bover-Arnal et al., 2009 *versus* Pomar and Haq, 2016 and Pomar, 2020) regarding the sequence-stratigraphy of the Aptian platform-to-basin transition area of Las Mingachas located at the western margin of the Maestrat Basin. Key outcrops and all geological features and fossil determinations relevant to the interpretations reported herein are illustrated to provide rigorous evidence and to avoid any misunderstanding on the interpretations of the features observed. The results and interpretations may be of relevance to those studying carbonate platforms and relative sea-level changes of glacio-eustatic magnitude, not only for the Cretaceous, but also for other periods in the Earth's history such as the late Paleozoic or Quaternary.

2. Geological setting

The outcrops studied are located in the eastern Iberian Chain (eastern Iberian Plate; Fig. 1A), which corresponds to an intraplate fold-and-thrust belt mainly resulting from the contractional inversion of the Late Permian-Maastrichtian Iberian Rift System (Álvaro et al., 1979; Salas et al., 2001; Guimerà et al., 2004; Nebot and Guimerà, 2016). Mesozoic normal faults had different orientations, mainly NW-SE, E-W and NE-SW: the boundaries of the Maestrat basin were defined by them (Fig. 1B). This tectonic inversion took place during the late Eocene-early Miocene contraction because of the convergence between the Iberian, African and Eurasian plates (Alpine orogeny) (Guimerà, 1994, 2018).

The Aptian stratigraphic intervals analyzed were deposited on the northwestern margin of the Alpine Tethys Ocean, within the Maestrat Basin (Figs. 1A-B), a rapidly subsiding basin, which was part of the Iberian Rift System (Salas and Casas, 1993; Salas et al., 2001). This basin, as well as other north-eastern Iberian basins such as Garraf, Columbrets, South-Iberian and Cameros (e.g., Salas et al., 2010), developed as a result of two rifting cycles (García-Senz and Salas, 2011; Salas et al. in Martín-Chivelet et al., 2019). These Kimmeridgian-early Berriasian and Barremian-early Albian rifting cycles resulted respectively from the opening of the North Atlantic and the Bay of Biscay domains (Salas et al., 2010).

During these rifting episodes, continental to marine sedimentation occurred in several subsiding zones separated by sedimentary thresholds or major normal faults, which structured the Maestrat Basin into different sub-basins (Fig. 1B; Salas et al. in Martín-Chivelet et al., 2019). In depocentral areas, the Upper Jurassic-Lower Cretaceous succession is >1.5 km thick, and more than 4 km in La Salzedella Sub-basin (Fig. 1B).

The study areas are located in the western marginal part of the Maestrat Basin; the Galve Sub-basin (Figs. 1B-C). The Galve Sub-basin was structured during the Early Cretaceous into half-graben structures mainly related to synsedimentary ENE-WSW normal listric faulting (Fig. 1C; Guimerà and Salas, 1996; Simón et al., 1998; Liesa et al., 2006). The rocks investigated crop out along two Cenozoic folds: the Miravete anticline (striking NNW-SSE) and the Camarillas syncline (striking NNE-SSE in the north and NNW-SSE in the south) to the West of the latter (Fig. 1C). The Miravete anticline has been recently interpreted as a diapiric structure that grew during the Jurassic and Early Cretaceous and acquired its present shape during a halokinetic final stage of rejuvenation related to the Alpine (Cenozoic) contraction (Vergés et al., 2020). To the West of the Miravete anticline, the Barremian-Aptian succession is thicker, and the marine facies indicate slightly deeper depositional environments than those reported from the eastern limb of this anticline structure (Simón et al., 1998; Bover-Arnal et al., 2010).

The uppermost Barremian-Aptian sedimentary record of the Galve Sub-basin is summarized in Fig. 2. From oldest to youngest, the lithostratigraphic units correspond to (i) the marine upper Barremian sandstones, sandy-limestones and limestones with *Palorbitolina lenticularis* of the Xert Formation, (ii) the uppermost Barremian-lower Aptian basinal marls and limestones with *P. lenticularis*, ammonoids, nautiloids and *Lithocodium aggregatum* of the Forcal Formation, (iii) the platform carbonates with rudists and corals of the upper lower Aptian Villarroya de los Pinares Formation, and finally (iv) the uppermost lower Aptian-upper Aptian (lowermost Albian?) marine marls, limestones with rudists and corals, and siliciclastics of the Benassal Formation (Martín-Martín et al., 2013; Bover-Arnal et al., 2016).

The uppermost lower Aptian and lower upper Aptian subaerial unconformities documented in the Galve Sub-basin were recorded within the Villarroya de los Pinares and Benassal formations, respectively (Fig. 2). Moreover, the subaerial incision cutting downwards the Villarroya de los Pinares Formation reported by Bover-Arnal et al. (2015) in the outcrop of La Serna, which is located in the south-central part of the Galve Sub-basin (Figs. 1B-C), will be also considered in the discussion of the paper. A further published example of an outcrop exhibiting evidence of major sea-level fall during the Aptian located within the Morella Sub-basin near the town of Morella (Fig. 1B; see Bover-Arnal et al., 2014) will be also reviewed and discussed. The Aptian succession of the Morella Sub-basin is similar to that developed in the Galve Sub-basin (see Canérot et al., 1982; Salas, 1987; Fig. 2).

3. Materials, methods and outcrops studied

The sedimentology, petrology, palaeontology and sequence stratigraphy of two Aptian stratigraphic intervals with different ages were examined in well-exposed outcrops of the Galve Sub-basin that recorded erosional or deeply incised subaerial unconformities. The upper lower Aptian succession (first case study) was analysed in four outcrops: Las Mingachas (latitude: 40.577219444444445, longitude: -0.7118944444444444), Barranco de la Canal (latitude: 40.616061111111115, longitude: -0.7493333333333333), Campillo Bajo (latitude: 40.609741666666665, longitude: -0.7447777777777778) and Camino de Camarillas (latitude: 40.602875000000004, longitude: -0.7561333333333333) (Fig. 1C). They all are located near the towns of Camarillas (Comarca de Comunidad de Teruel) and Miravete de la Sierra (Comarca de El Maestrazgo). The second case study of lower upper Aptian age was studied in the outcrop of Loma de Camarillas (latitude: 40.59986388888889, longitude: -0.7212416666666667), which is also located near Miravete de la Sierra (Fig. 1C).

The Aptian succession of the Galve Sub-basin was previously analysed by various authors (Weisser, 1959; Vennin and Aurell, 2001; Bover-Arnal et al., 2009, 2010, 2011, 2012, 2015, 2016; Embry et al., 2010; Moreno-Bedmar et al., 2010; Skelton et al., 2010; Peropadre et al., 2013; Bonin et al., 2016; Gili et al., 2016; Pomar and Haq, 2016; Vergés et al., 2020; Gratacós et al., 2021). For the present paper, only key

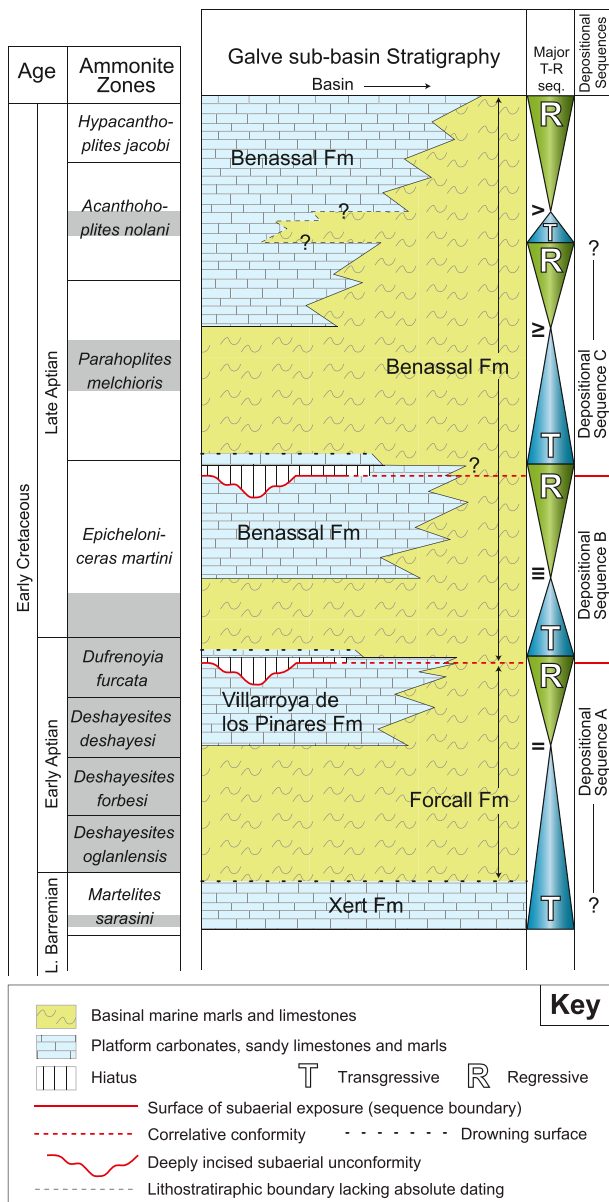


Fig. 2. Chrono-stratigraphic chart for the latest Barremian-Aptian of the Galve Sub-basin. The chrono-stratigraphic chart includes major transgressive-regressive sequences (modified from Bover-Arnal et al., 2016) and depositional sequences interpreted in this study. The ammonoid zonation is taken from Reboulet et al. (2018). The ammonite zones identified in the Maestrat Basin are highlighted in grey.

stratigraphic intervals including subaerial unconformities, or interpreted as forced regressive and transgressive deposits in previous works, have been revisited for further analysis. The study site of Loma de Camarillas (Fig. 1C) is described here for the first time.

Panoramic photographs and close-up views of the outcrops were used to map the facies, stratigraphic geometries and key sequence-stratigraphic surfaces such as major unconformities. Two stratigraphic logs, 12.5 and 42 m thick, were measured and analysed bed-by-bed in Las Mingachas and Loma de Camarillas sites, respectively (Fig. 1C). Description of sedimentary facies and palaeontological determinations was performed on 141 thin sections made from samples collected in the five outcrops studied. Carbonate rock textures follow the classifications of Dunham (1962) and Embry and Klován (1971), whereas the sequence stratigraphic analysis follows the terminology proposed by Catuneanu et al. (2009).

4. Results and discussion

4.1. Late early Aptian case study

4.1.1. Las Mingachas

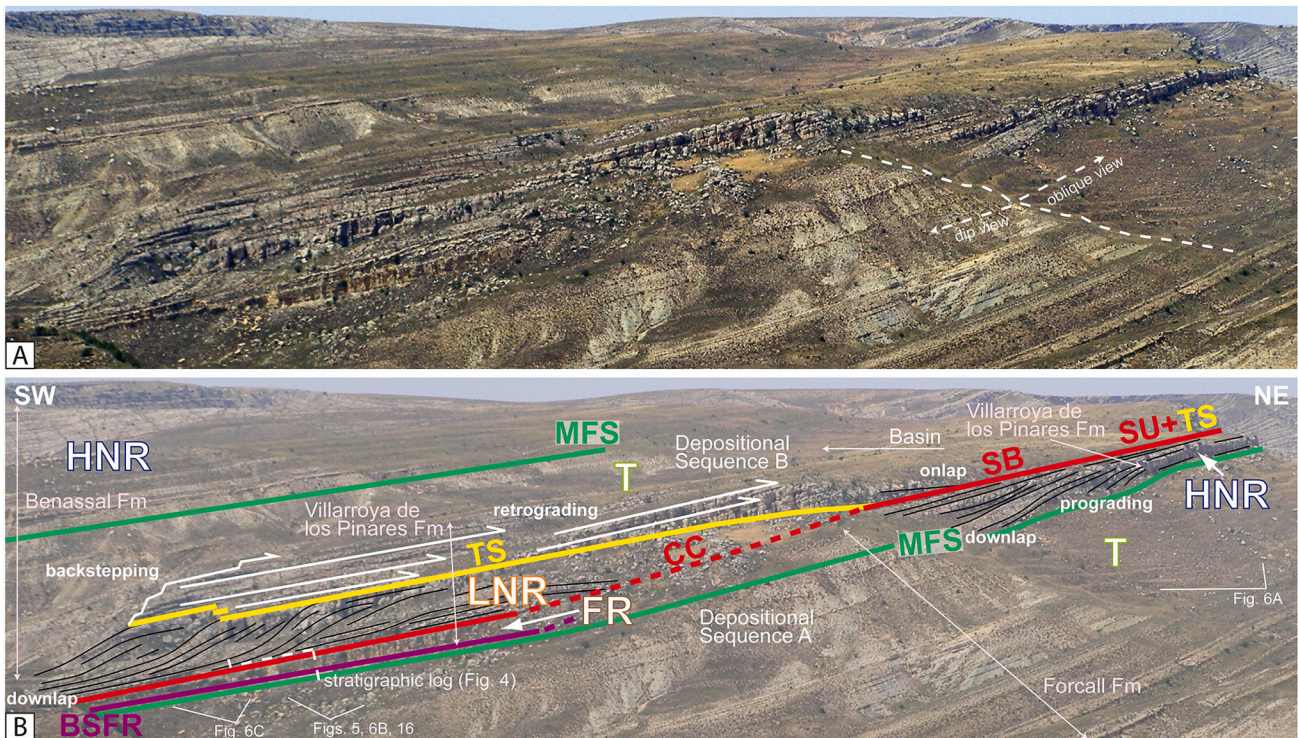
Las Mingachas outcrop (Fig. 1C) was firstly studied by Bover-Arnal et al. (2009, 2010, 2011, 2012) and the succession was interpreted to represent a carbonate platform-to-basin transition area. It covers two depositional sequences (A and B), which are separated by a subaerial unconformity passing basinwards to its marine correlative conformity (Fig. 3). The older depositional sequence (Depositional Sequence A) includes a forced regressive wedge belonging to the Villarroya de los Pinares Formation (Figs. 3-5).

The present study reviews and expands the sequence-stratigraphic analysis carried out in Las Mingachas by Bover-Arnal et al. (2009) (Figs. 3 and 6). This revision focuses on the forced regressive unit *sensu* Bover-Arnal et al. (2009) and consists of new and detailed sedimentological, petrological and palaeontological analyses (Figs. 7-8), including an original log (Fig. 4) and outcrop photographs with the sequence-stratigraphic interpretation (Figs. 5-6).

4.1.1.1. Description of the sedimentary succession. In the distal parts of the carbonate system studied, the first 2 m of the succession (Figs. 3A-B and 4-5) consist of marls (Fig. 7A), and locally bioturbated marly-limestones and limestones with matrix-supported (Fig. 7B) to packstone textures, dominated by large-sized (diameter > 3 mm) discoidal *Palorbitolina lenticularis* (Fig. 7C). This interval, which belongs to the Forcall Formation (Fig. 2), contains other skeletal components such as *Praeorbitolina cormyi*, *Choffatella decipiens*, textularids, lituolids, miliolids, calcareous dinoflagellate cysts, *Dufrenoyia* sp. ammonoids, other molluscs, sponge spicules, brachiopods, serpulids, echinoids and crustacean debris. Peloids and silt-sized quartz are common non-skeletal components (Fig. 4).

The 2 to 4.1 m interval succession corresponds to the uppermost part of the Forcall Formation and contains thin marl intervals and bioturbated marly-limestones with wackestone to packstone textures rich in large-sized (diameter > 3 mm) discoidal *P. lenticularis* (Figs. 4 and 7D). *P. cormyi* was also found (Fig. 7E). In this interval, oysters, encrusting foraminifera and benthic foraminifera such as miliolids, *C. decipiens* and lituolids become more abundant, whereas calcareous dinoflagellate cysts and sponge spicules become scarcer or are even absent. Two *Dufrenoyia* sp. ammonite specimens were found (Figs. 4 and 7F). Noteworthy is that this interval also recorded the first scarce to common occurrence of rudist fragments (Fig. 8A), bryozoans, corals and *Permo-calculus* (Fig. 8B). Besides fragmentation, the coral, rudist and *Permo-calculus* debris observed also show significant abrasion (Figs. 8A-B). Other taphonomic features that occur are encrustation, mainly by encrusting foraminifera, peyssoneliacean algae and *Lithocodium aggregatum*, and extensive bioerosion on large skeletal components (diameter > 1 mm). Non-skeletal components such as peloids and silt-sized quartz grains are common (Fig. 4). This interval (Figs. 4-5) passes landwards (northwards) to topographically higher, aggrading-prograding platform carbonates with downlap stratal terminations of the Villarroya de los Pinares Formation (Figs. 3 and 6A). These limestones are distinguished by floatstone and rudstone textures which include corals and rudists in life position (Bover-Arnal et al., 2009). The top of the preserved aggrading platform carbonates is located at a topographic height of c. 1362 m (Fig. 6A).

Basinwards, at metre 4.1 in the logged section, a limestone bed with a sharp base (Fig. 5) and burrow structures, marks a significant change in sedimentary bedding, lithology, textural characteristics, and biota (Fig. 4). Below this bed, signs of subaerial exposure were not identified. Above, and until 8.1 m in section, the succession displays highly-bioturbated marly-limestones with a packstone-grainstone texture, but also marls, and large-scale low-angle cross-bedded limestones exhibiting



Key

- HNR: Highstand Normal Regressive
- FR: Forced Regressive
- LNR: Lowstand Normal Regressive
- T: Transgressive
- BSFR: Basal Surface of Forced Regression
- SB: Sequence Boundary
- TS: Transgressive Surface
- MFS: Maximum Flooding Surface
- CC: Correlative Conformity
- SU: Subaerial Unconformity

Relative sea level

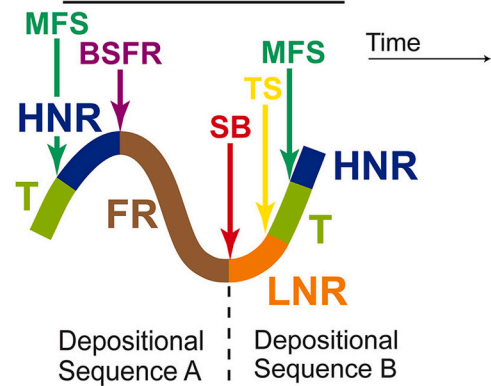


Fig. 3. Las Mingachas. A) Panoramic view of a platform-to-basin transition. Width of image = c. 550 m. B) Interpretation of Fig. 3A including the lithostratigraphic units, the sequence stratigraphic framework, and the location of Figs. 5, 6A-C and 16 and the stratigraphic log shown in Fig. 4. Note how the forced regressive wedge interpreted is located topographically below the highstand prograding platform of Depositional Sequence A, and how this basin floor component is downlapped by an overlying prograding lowstand platform belonging to Depositional Sequence B. Modified from Bover-Arnal et al. (2009, 2011). C) Not to scale two-dimensional schematic model showing the Aptian platform development, lithofacies architecture and sequence stratigraphic evolution from the proximal platform settings of Camarillas to the platform-to-basin transition area of Las Mingachas. Based on Bover-Arnal et al. (2009) and modified from Gili et al. (2016). The situation of the conceptual cross-section A-A' is indicated in Fig. 1C.

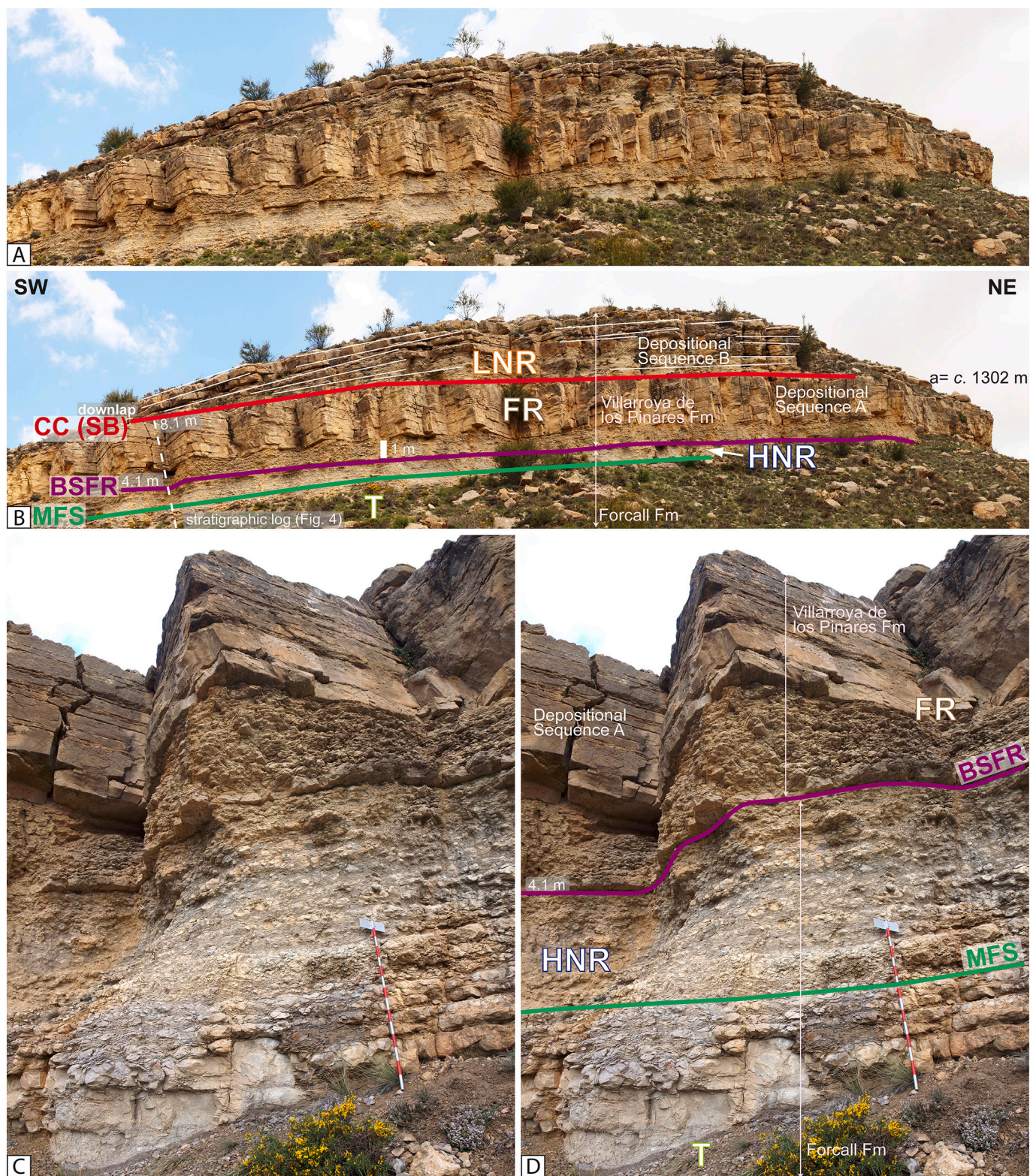
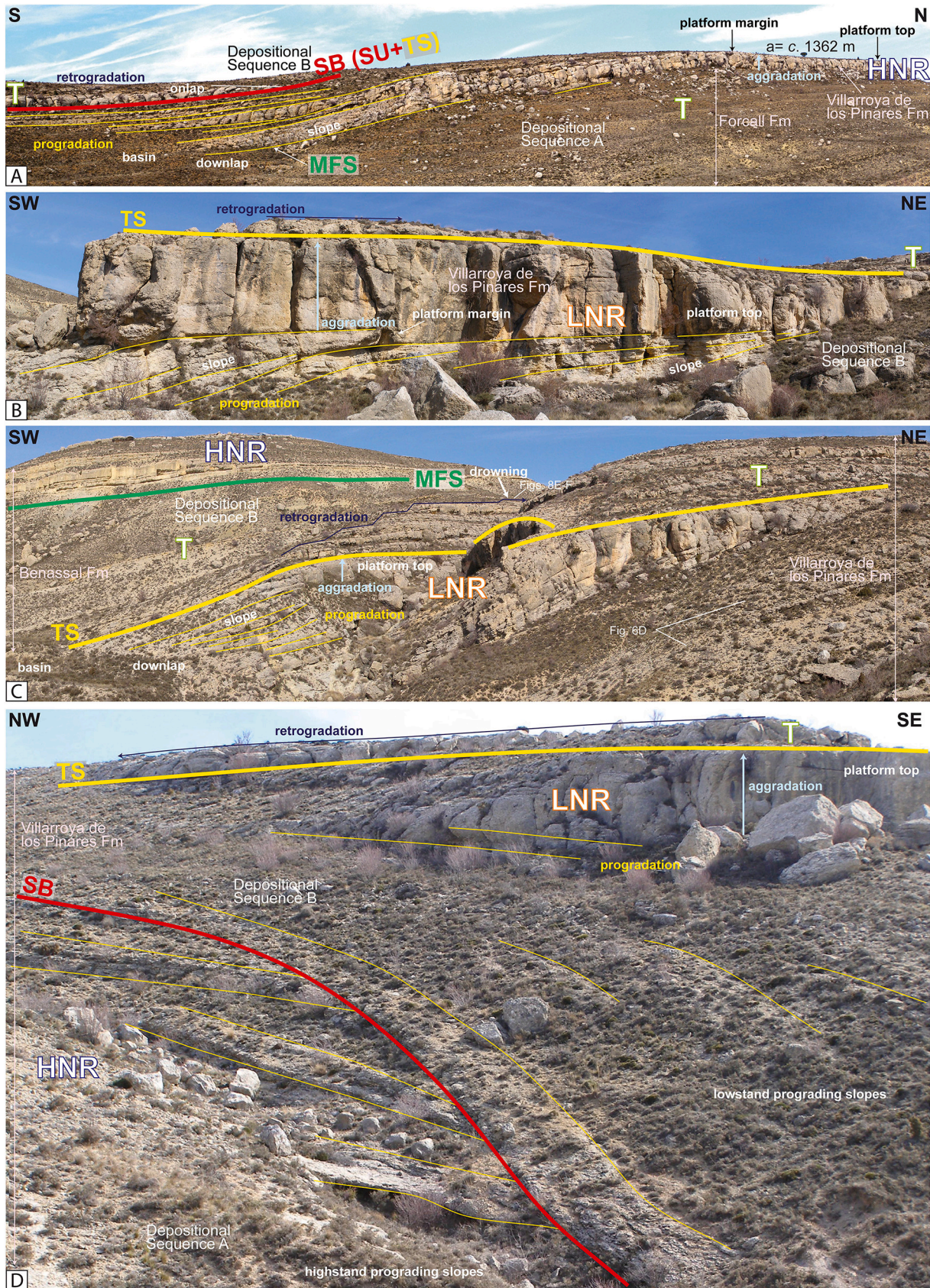


Fig. 5. Las Mingachas. A) Outcrop photograph of the sedimentary wedge interpreted as a forced regressive unit. B) Interpretation of Fig. 5A including the lithostratigraphic units, the sequence stratigraphic framework, and the stratigraphic log shown in Fig. 4. Note the sharp nature of the interpreted basal surface of forced regression and correlative conformity (sequence boundary). a = altitude. Inset: scale bar = 1 m. Modified from Bover-Arnal et al. (2009). C) Outcrop view of the lower part of the sedimentary log shown in Fig. 4. D) Interpretation of Fig. 5C including the lithostratigraphic units and the sequence stratigraphic framework. Jacob's staff = 1.5 m. See Fig. 3 for key.



(caption on next page)

Fig. 6. Las Mingachas. Sequence-stratigraphic interpretations are after Bover-Arnal et al. (2009). See Fig. 3 for key. See also Bover-Arnal et al. (2009) for uninterpreted images of the outcrop views. A) Photomosaic of the north-eastern part of Las Mingachas showing the aggrading, prograding and downlapping platform carbonates interpreted as a highstand normal regressive unit. a = altitude. Width of image = c. 300 m. See Fig. 3 for location of the photomosaic. B) Outcrop view of the prograding-aggrading platform interpreted as a lowstand normal regressive unit, which crops out in the south-western part of Las Mingachas area. Width of image = c. 40 m. See Fig. 3 for location. C) Panoramic view of the prograding and aggrading lowstand normal regressive platform located in the south-western part of Las Mingachas area. Note how above the TS the carbonates are stacked in a retrograding pattern. Width of image = c. 120 m. See Fig. 3 for location. D) Outcrop view of the erosional unconformity (sequence boundary) between the highstand slopes of Depositional Sequence A and the lowstand slopes of Depositional Sequence B cropping out in the south-western part of Las Mingachas area. The view is from the other side of the platform from 6B. Width of image = c. 45 m. See Fig. 6C for location.

(Benassal Formation) consists of platform carbonates with rudists, corals and nerineids (Figs. 3A-B and 6C).

4.1.1.2. Palaeoenvironmental and sequence-stratigraphic interpretation.

At the north-eastern part of Las Mingachas (Fig. 3), the rudist- and coral-bearing platform carbonates of the Villarroya de los Pinares Formation are characterized by an aggrading and succeeding prograding stacking pattern (Fig. 6A). In the SW direction (towards the basin), these limestone beds, which are slightly inclined relative to regional dip, show downlap stratal terminations. They overlie and laterally pass over into the marls of the Forcall Formation (Figs. 3 and 6A). Based on the outcrop features, this carbonate unit can be interpreted as a highstand normal regressive (HNR) platform. The inclined beds correspond to an oblique view of the prograding platform slopes with apparent dip angles (Fig. 6A). Slope progradation is towards the west-southwest, and therefore the true dip angles are higher. The horizontal aggrading level corresponds to platform top deposits (Figs. 3A-B and 6A). Hence, the stratigraphic succession described above and shown in Fig. 6A matches a platform top-to-basin transition with a preserved platform margin, which lacks barrier facies.

Here, the base of the highstand normal regressive carbonates is marked by a downlap surface onto the transgressive marly succession of the Forcall Formation. This downlap surface limiting deeper basal marls below from limestones with rudists and corals above is regarded as the maximum flooding surface (MFS) of Depositional Sequence A (Figs. 3 and 6A). In seismic sequence-stratigraphy, the maximum flooding surface is commonly placed at the downlap surface of normal regressive prograding clinoforms above deeper, transgressive (T) deposits (e.g., Catuneanu et al., 2011; Catuneanu, 2019).

Basinwards, in the south-western part of Las Mingachas outcrop (Figs. 3 and 5), abraded and fragmented remains of rudists (Fig. 8A), corals and *Permocalculus* (Fig. 8B) occur in the uppermost part of the Forcall Formation (Fig. 4). Although these marly deposits are characterized by the presence of well-preserved tests of *P. lenticularis* and *P. cornyi*, the occurrence of the shallower-water skeletal fragments becomes prominent above metre 2 in the logged stratigraphic section (Fig. 4). The pre-burial taphonomic features such as fragmentation and abrasion exhibited by the shallower-water grains suggest sediment-transport (see e.g., Beavington-Penney, 2004), and are therefore indicative of basinwards shedding of platform top carbonates due to the progradation of the carbonate system. Accordingly, the uppermost part of the Forcall Formation (between metres 2 and 4.1 in Fig. 4) is interpreted to represent the basal marly counterpart of the above-mentioned highstand platform of the Villarroya de los Pinares Formation located landwards, in a higher topographic position (Figs. 3 and 6A). This basal equivalent is thus construed as a highstand normal regressive unit (Figs. 3–5). The maximum flooding surface is placed at metre 2, just below the first significant arrival in basal settings of fragments of rudists, corals and *Permocalculus* (Fig. 4). The marly succession below the maximum flooding surface is interpreted as a transgressive deposit (Figs. 3–5).

At metre 4.1 (Fig. 4), the succession passes from the matrix-supported marly limestones of the uppermost Forcall Formation to well-stratified packstone-grainstone limestones of the Villarroya de los Pinares Formation indicating deposition under higher-energy conditions than the underlying marly strata. It is also worth noting that the

lowermost, non-basal part of the Villarroya de los Pinares Formation (between metres 4.2 and 5.3 in Fig. 4) exhibits a nodular aspect that resulted from intense bioturbation (Fig. 5). Above metre 4.1, *P. lenticularis* becomes smaller sized and scarcer, sponge spicules and calcareous dyncocysts disappear, whereas small-sized conical *Orbitolinopsis* shows its first occurrence and dominates the succession together with coral and *Permocalculus* debris until metre 8.1 (Figs. 4 and 8C-D). *Orbitolinopsis* thrived in more shallower platform environments compared to larger-sized discoidal *P. lenticularis* (see e.g., Champetier and Moullade, 1970; BouDagher-Fadel and Price, 2019). *M. lugeoni* (Fig. 8C) and intraclasts (Fig. 8D) also occur for the first time and are common components throughout this latter stratigraphic interval (Fig. 4). Small *Marinella lugeoni* lumps such as those observed in the lower part of the Villarroya de los Pinares Formation in Las Mingachas (Figs. 4–5 and 8C) were interpreted by Granier and Dias-Brito (2016) as having an epiphytal behaviour and thus, would constitute palaeoenvironmental indicators of well-illuminated shallow platform settings. In comparison to the basal fossil content identified for the Forcall Formation (Fig. 4), the biota recorded within this higher-energy unit mark a change in carbonate factory and indicates deposition in shallower and better-illuminated water settings, and thus an abrupt decrease in water depth which was the result of a drop in sea level.

Carbonate grains forming the packstone-grainstone wedge were sourced from organisms thriving locally or in nearby settings during sea-level fall. The occurrence of abundant intraclasts (Figs. 4 and 8D) indicates intrabasinal erosion and reworking of lithified material. Eroded skeletal fragments from the subaerially exposed highstand platform were also likely transported and redeposited into this regressive deposit.

The higher-energy regressive unit (from metre 4.1 to metre 8.1 in Fig. 4) constitutes a detached sedimentary wedge which does not show a bedding, textural or biotic similarity with lateral equivalent, underlying or overlying strata in Las Mingachas (Fig. 3). This regressive sedimentary wedge crops out mostly in two dimensions along c. 240 m, and was accumulated basinwards of highstand prograding slopes (Fig. 3). The top of the sedimentary wedge is located in a lower topographic level (c. 1302 m altitude; Figs. 3 and 5) compared to the top of the preserved part of the highstand normal regressive platform (c. 1362 m altitude; Figs. 3 and 6A). The present-day regional (post-depositional) dip of the strata here is c. 9° (Vergés et al., 2020), which must account for some altitude difference. Landwards, in a northern direction, the highstand normal regressive platform top is continuously exposed for nearly 8 km and exhibits deeply incised valleys (Figs. 9–10), which are indicative of a forced regression. Accordingly, the detached grainstone wedge is interpreted as a forced regressive (FR) unit deposited in a basal position during sea-level fall (Figs. 3–5). The sharp surface located at the base of this basin floor component would then correspond to a basal surface of forced regression (BSFR) *sensu* Hunt and Tucker (1992) (Figs. 3–5). In this regard, the top of the underlying highstand basal deposits of the Forcall Formation lacks any evidence of subaerial exposure (Fig. 5).

The forced regressive wedge is downlapped by the slope strata of a carbonate platform with a reduced size of its shallow-water realm. The platform exhibits a progradational stacking pattern followed by an aggradational behaviour (Figs. 3A-B, 5A-B and 6B-D). The stacking patterns shown agree with a lowstand normal regressive (LNR) carbonate platform, which flourished during subsequent sea-level rise after a

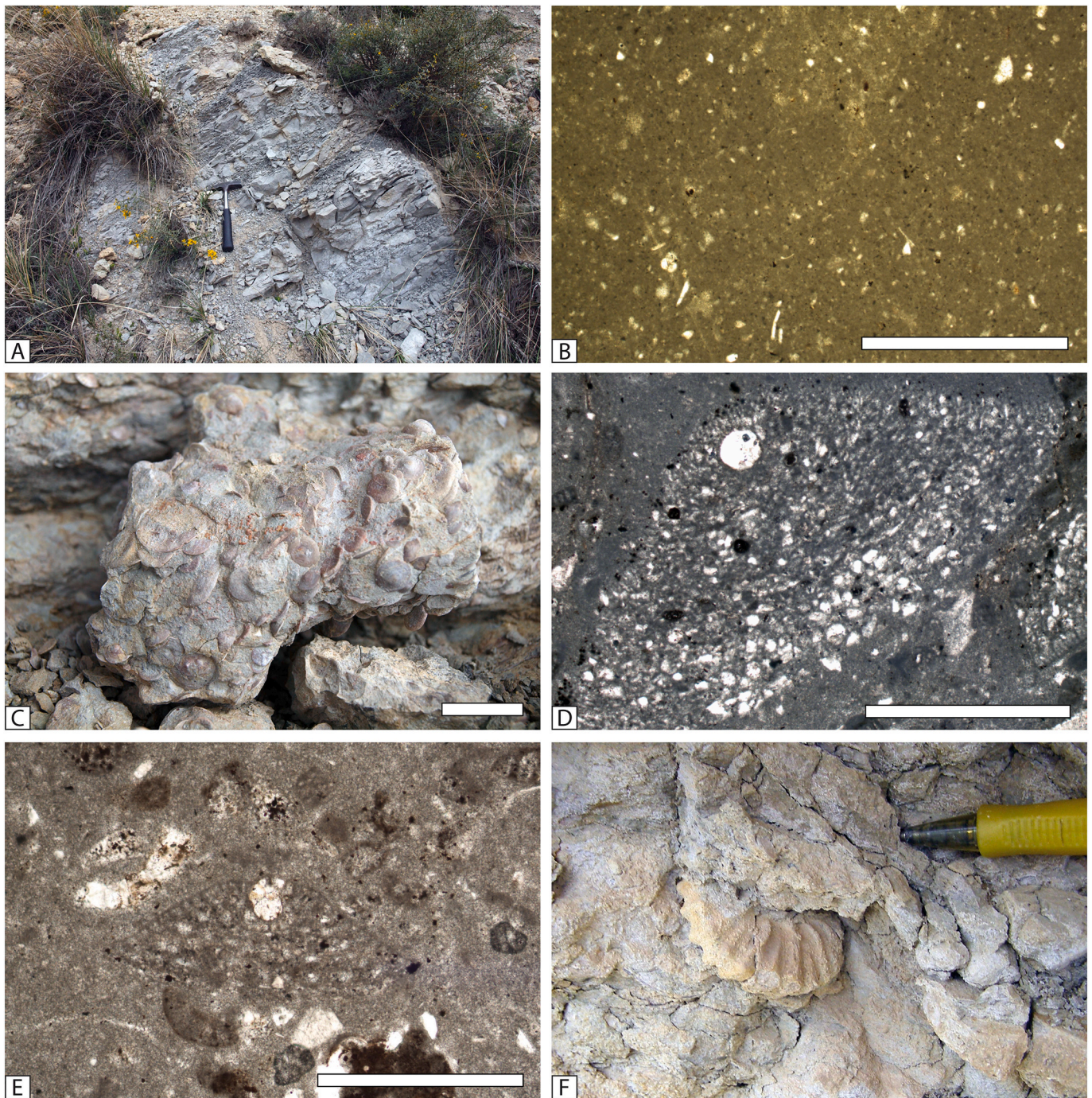


Fig. 7. Las Mingachas. A) Outcrop view of the basal transgressive marls of the Forcall Formation (lower Aptian). Depositional Sequence A. Hammer = 32 cm. B) Matrix-supported texture with fragments of molluscs. Transgressive deposits of the Forcall Formation (lower Aptian). Depositional Sequence A. Scale = 1 mm. C) Packstone texture with *Palorbitolina lenticularis* of the upper, transgressive part of the Forcall Formation (lower Aptian). Depositional Sequence A. Scale = 1 mm. D) Photomicrograph of a specimen of *Palorbitolina lenticularis* showing the embryonic apparatus. Highstand normal regressive marly-limestones of the Forcall Formation (lower Aptian). Depositional Sequence A. Scale = 1 mm. E) Photomicrograph of a specimen of *Praeorbitolina cormyi* showing the embryonic apparatus. Highstand normal regressive deposits of the Forcall Formation (lower Aptian). Depositional Sequence A. Scale = 1 mm. F) *Dufrenoyia* sp. Highstand normal regressive marly-limestone deposits of the Forcall Formation (lower Aptian). Depositional Sequence A. Visible part of pencil = 3.9 cm. See Fig. 4 for locations.

forced regression (Figs. 3 and 6B-D). The small lowstand platform progrades in a south-southwest direction. Noteworthy is that the passage from platform top to slope settings lacks a barrier margin and is only marked by a change of bed dip and facies (Figs. 6B-C; see Bover-Arnal et al., 2009). The lowstand platform is also located basinwards, in a lower topographic position than the highstand normal regressive platform situated in the north-eastern part of Las Mingachas (Fig. 3).

The sharp surface at the top of the forced regressive grainstone

wedge that it is downlapped by lowstand slope deposits marks the lowest point of relative sea-level (Figs. 3 and 5A-B), and thus corresponds to a sequence boundary (SB) *sensu* Hunt and Tucker (1992). Given that this basin floor component was never subaerially exposed, the sequence boundary is classified as a marine correlative conformity (CC) (Figs. 3-4 and 5A-B). The correlative conformity passes landwards into a subaerial unconformity (SU) (Figs. 3, 6A and 9-11A). In Las Mingachas, this sequence boundary is also expressed by the truncation

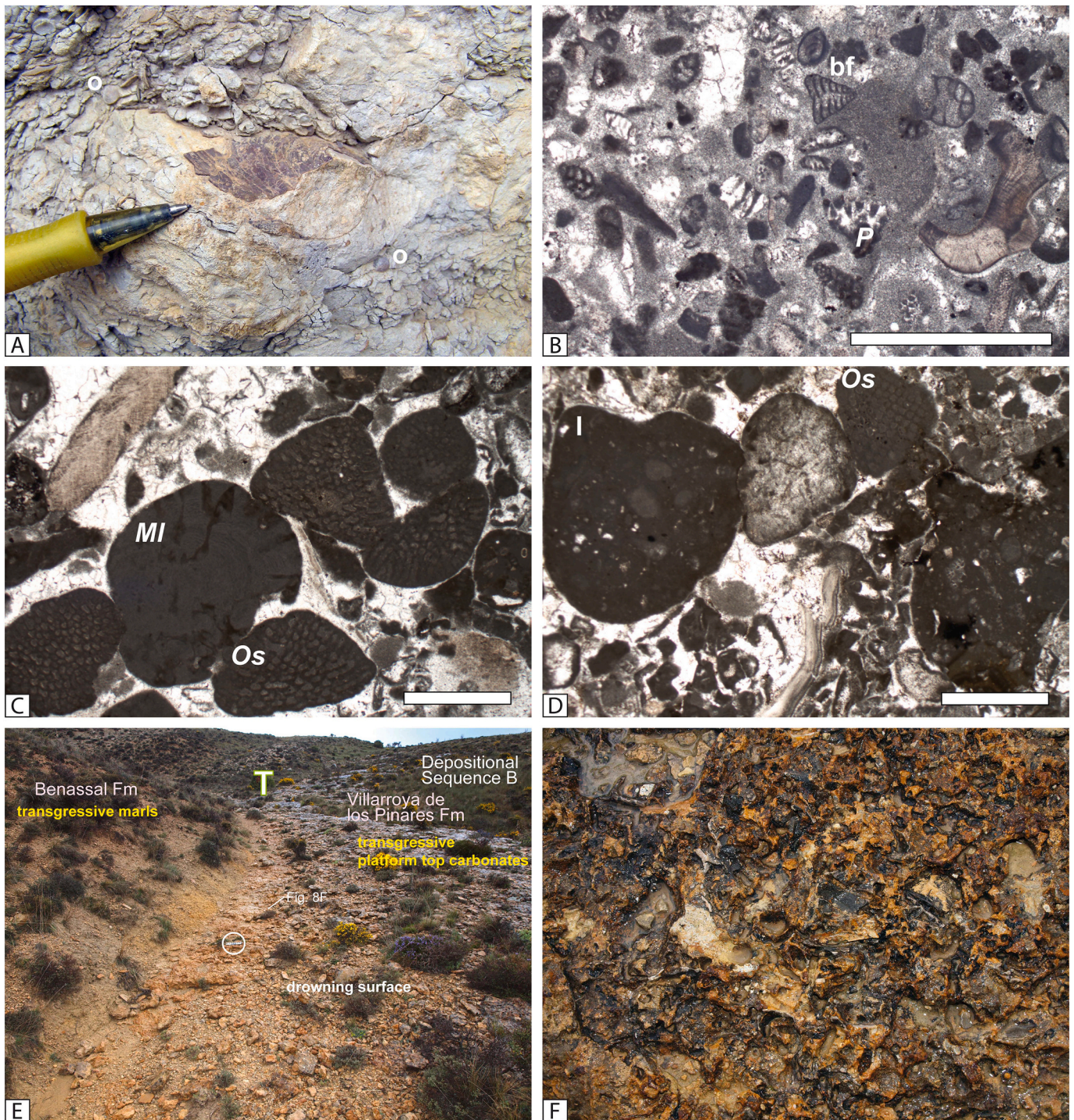


Fig. 8. Las Mingachas. A) Detail of a poorly preserved rudist section present in the highstand normal regressive marly-limestones of the Forcall Formation (lower Aptian). Note the presence of orbitolinids (o). Depositional Sequence A. Visible part of pencil = 3 cm. B) Packstone of benthic foraminifera (bf) and abraded fragments of *Permolcalculus* (P) belonging to the highstand normal regressive deposits of the Forcall Formation (lower Aptian). Depositional Sequence A. Scale = 1 mm. C) Grainstone texture containing specimens of *Orbitolinopsis* (Os) and a section of *Marinella lugeoni* (MI) of the middle part of the forced regressive wedge. Villarroya de los Pinares Formation (lower Aptian). Depositional Sequence A. Scale = 1 mm. D) Microphotograph of the forced regressive deposits exhibiting a grainstone texture with intraclasts (I) and a specimen of *Orbitolinopsis* (Os). Villarroya de los Pinares Formation (lower Aptian). Depositional Sequence A. Scale = 1 mm. See Fig. 4 for locations. E) Outcrop view of the transgressive marls of the lower part of the Benassal Formation overlying drowned transgressive platform top carbonates belonging to the Villarroya de los Pinares Formation (uppermost lower Aptian). Depositional Sequence B. Encircled ruler = 15 cm. See Figs. 3 and 6C for key and location, respectively. F) Close-up view of the drowning surface located at the top of the transgressive platform carbonates of the Villarroya de los Pinares Formation (uppermost lower Aptian). This ferruginous and perforated surface corresponds to a hardground. Depositional Sequence B. Width of image = c. 25 cm. See Figs. 6C and 8E for location.

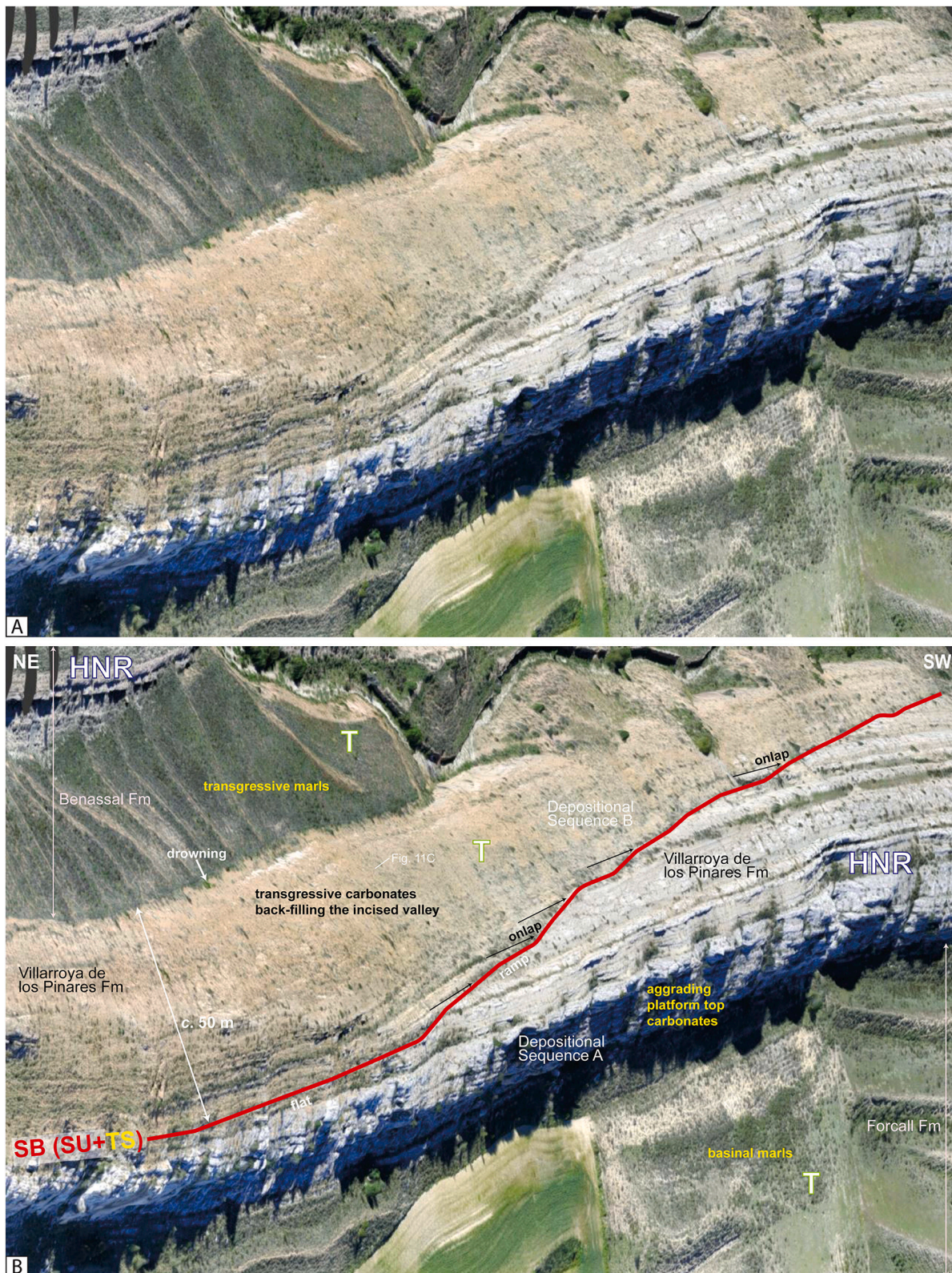


Fig. 9. Barranco de la Canal. A) Drone-based photogrammetric model of the deeply incised erosional surface bounding highstand platform top carbonates of Depositional Sequence A from the overlying transgressive limestones, which back-fill an incised valley, of Depositional Sequence B above. B) Interpretation of Fig. 9A including the lithostratigraphic units and the sequence-stratigraphic interpretation after Bover-Arnal et al. (2009). Note the stepped nature of the incision surface. Note also the drowning of the higher-energy transgressive unit of the uppermost Villarroya de los Pinares Formation and how it is buried by marls of the lower part of the Benassal Formation. See Figs. 3 and 1C for key and location, respectively. The drone-based photogrammetric model is courtesy of Riccardo Rocca and available at http://riccardorocca.github.io/home/Camarillas_Platform.html, accessed 11 September 2021).

Fig. 10. Campillo Bajo. A) Panoramic photomosaic showing the composite sequence boundary (SU + TS) between depositional sequences A and B at the southern cliff of a small river, which flows across the Campillo Bajo area. B) Interpretation of Fig. 10A including the lithostratigraphic units and the sequence-stratigraphic interpretation after Bover-Arnal et al. (2010). Note the stepped nature with flats and ramps of this deeply incised erosional surface and the onlap stratal terminations of transgressive limestones onto surface slopes. Note also the drowning cover of the transgressive carbonates by marls of the Benassal Formation. See Figs. 3 and 1C for key and location, respectively. Use the depth of the palaeovalley for scale. C) View of the composite sequence boundary (SU + TS) between depositional sequences A and B cropping out in the northern side of a small river, which flows across the Campillo Bajo area. D) Interpretation of Fig. 10C including the lithostratigraphic units and the sequence-stratigraphic interpretation after Bover-Arnal et al. (2011). Note the flat-and-ramp geometry exhibited by this surface and how the transgressive deposits onlap the ramps and overlie the flats. Encircled geologist for scale. See Figs. 3 and 1C for key and location, respectively.

of highstand prograding slopes, which are overlain by lowstand prograding slopes (Fig. 6D). The sequence boundary separates two depositional sequences: A and B (Figs. 3–4, 5A–B and 6A, D).

Above the aggrading limestones of the upper part of the lowstand normal regressive unit, platform carbonates are stacked in a retrograding pattern (Figs. 3 and 6). The change from aggradation to retrogradation is marked by a transgressive surface (TS) (Figs. 3 and 6), which locally exhibits borings and ferruginous stains (Bover-Arnal et al., 2009). These backstepping platform carbonates are part of the Villarroya de los Pinares Formation and basinwards and upwards pass over into a succession with transgressive basinal marls of the lower part of the Benassal Formation (Fig. 6C). The retrograding carbonate system of Depositional Sequence B onlaps the slopes of the highstand normal regressive platform of Depositional Sequence A (Figs. 3 and 6A). The transgressive surface superposed onto the subaerial unconformity thus is a composite sequence boundary (Figs. 3 and 6A). Locally, a perforated and ferruginous hardground surface marks the drowning (*sensu* Schlager, 1981) of the transgressive carbonates (Figs. 6C and 8E–F).

The hardgrounds developed within this transgressive stratigraphic interval are local to regional features and thus, they were formed and controlled by local to regional factors. The time involved in the hardground formation is unknown as it is below the resolution of ammonite biostratigraphy. The occurrence of Fe mineralizations, encrusting organisms and lithophagid bivalve borings on these surfaces indicates periods of suspended sedimentation or reduced sedimentation rates due to erosion and current activity (e.g., Shinn, 1969). The precipitation of Fe-oxides involves inorganic and microbial processes and commonly occurs during the hardground formation and the subsequent burial stage (see e.g., Christ et al., 2015). In the sedimentary record studied, hardground formation is linked to transgressive surfaces (Fig. 6C) or flooding pulses (Figs. 8E–F) and thus, to abrupt rises of relative sea level. The fact that the hardgrounds cap platform carbonate successions that are overlain by marl deposits points to drowning (Figs. 6C, 8E–F, 9, 10A–B and 11B). During early transgressive contexts, carbonate accumulation was reduced and restricted to very narrow areas (Figs. 6C, 9 and 10A–B). After a rapid and significant increase in water depth, and under such weakened conditions, the carbonate factory did not have enough growth potential to catch up or keep pace with the rate of sea-level rise.

The uppermost part of the marl interval of the Benassal Formation is characterized by the occurrence of isolated large colonial corals in growth position. The facies of scleractinian corals embedded in marls is indicative of slope settings (Bover-Arnal et al., 2012), which mark shallower waters than the underlying basinal marls. Consequently, the maximum flooding surface of Depositional Sequence B is thus interpreted to be at the base of this coral-rich marly level (Figs. 3A–B and 6C). Above, platform carbonates with rudists and corals also belong to the Benassal Formation, and flourished during the subsequent highstand stage of Depositional Sequence B (Figs. 3A–B and 6C).

4.1.2. Barranco de la Canal, Campillo Bajo and Camino de Camarillas

Proximal parts of the highstand normal regressive platform of Depositional Sequence A (Fig. 3) crop out in the surroundings of the town of Camarillas (Fig. 1C). Whereas in platform-to-basin settings (i.e., Las Mingachas), major sea-level fall was recorded as a forced regressive basin floor component (Figs. 3 and 5), in inner platform environments this drop in sea level is expressed as a subaerial unconformity cutting deeply into highstand platform top carbonates (Bover-Arnal et al., 2009,

2010, 2011).

The results of forced regression and subsequent sea-level rise in a proximal area of the upper lower Aptian carbonate system are characterized herein in three separate outcrops (Barranco de la Canal, Campillo Bajo and Camino de Camarillas; Fig. 1C), which show the same sedimentary architecture and evolution. The subsection takes another look at this subaerial unconformity cropping out in the environs of Camarillas (Fig. 1C) using an original drone-based photogrammetric model (Fig. 9). Furthermore, it re-examines the sequence-stratigraphic analysis performed by Bover-Arnal et al. (2009), and provides a characterization of the erosional surface (sequence boundary), as well as an illustrated facies analysis of the underlying and overlying deposits (Figs. 10–11).

4.1.2.1. Description of the sedimentary succession. Overlying the basinal marls with ammonoids and *P. lenticularis* of the Forcall Formation, there is a succession with aggrading platform top carbonates (Fig. 9) mainly characterized by floatstone to rudstone textures including scleractinian corals, gastropods, *Chondrodonta* and rudists such as *T. carinata*, *P. hadriani*, *Monopleura* sp., *C. parvula* and *Offneria* sp. (Bover-Arnal et al., 2010). The coral- and rudist-bearing limestone succession is part of the Villarroya de los Pinares Formation and is truncated and deeply incised by a subaerial unconformity displaying a flat-and-ramp erosional profile (Figs. 9–11A). To the North of Camarillas (Fig. 1C), the incision is around 50 m deep (Fig. 9), and more than 1.5 km in width. Peropadre et al. (2013) give a maximum depth of 57 m for this incision in Camarillas. To the South of Camarillas, the measured depth of the incision is lower (c. 15 m; Fig. 10A–B).

The erosional surface exhibits widespread dissolution of truncated skeletal components and palaeokarst with sedimentary infillings (Fig. 11D). Locally, bioclastic coarse infillings occur (Fig. 11E). In the Camino de Camarillas outcrop (Fig. 11A), the palaeokarst reaches down by around 1 m. Superimposed onto the subaerial unconformity there is a rockground with borings and ferruginous stains and crusts (Fig. 11F).

Above the erosional surface, the Villarroya de los Pinares Formation is made up of a succession of cross-bedded orange-coloured limestones (Fig. 9) with packstone to grainstone textures rich in oyster fragments (Fig. 11C). Locally, herringbone cross-stratification occurs (Fig. 11B). The cross-bedded limestones overlie the flats and onlap the ramps exhibited by the erosional surface (Figs. 9–11A). Besides oysters, fragments of other molluscs, *Permodaculus*, echinoids, crinoids, corals, as well as serpulids and tests of orbitolinids, *Choffatella*, miliolids and of other benthic foraminifera, are also common skeletal components in these higher-energy carbonates. Peloids, silt- to fine sand-sized quartz grains and intraclasts are also frequent. The limestones of the lower part of this oyster-bearing unit also include mud pebbles. The incised grey platform carbonates with rudists and corals, and the overlying orangish limestones with cross-bedding and oysters, show similar dip and dip directions (Figs. 9–11A).

The top of the cross-bedded limestone succession with oysters locally exhibits a hardground surface with a ferruginous crust and is overlain by the marls of the lower part of the Benassal Formation (Figs. 9 and 10A–B). At the Campillo Bajo site (Fig. 1C), unbound level-bottom populations of colonial corals are found embedded in the marls of the lowermost part of this lithostratigraphic unit. Above the marl succession, grey platform carbonates with corals, rudists and nerineid gastropods of the Benassal Formation were deposited (Fig. 9).

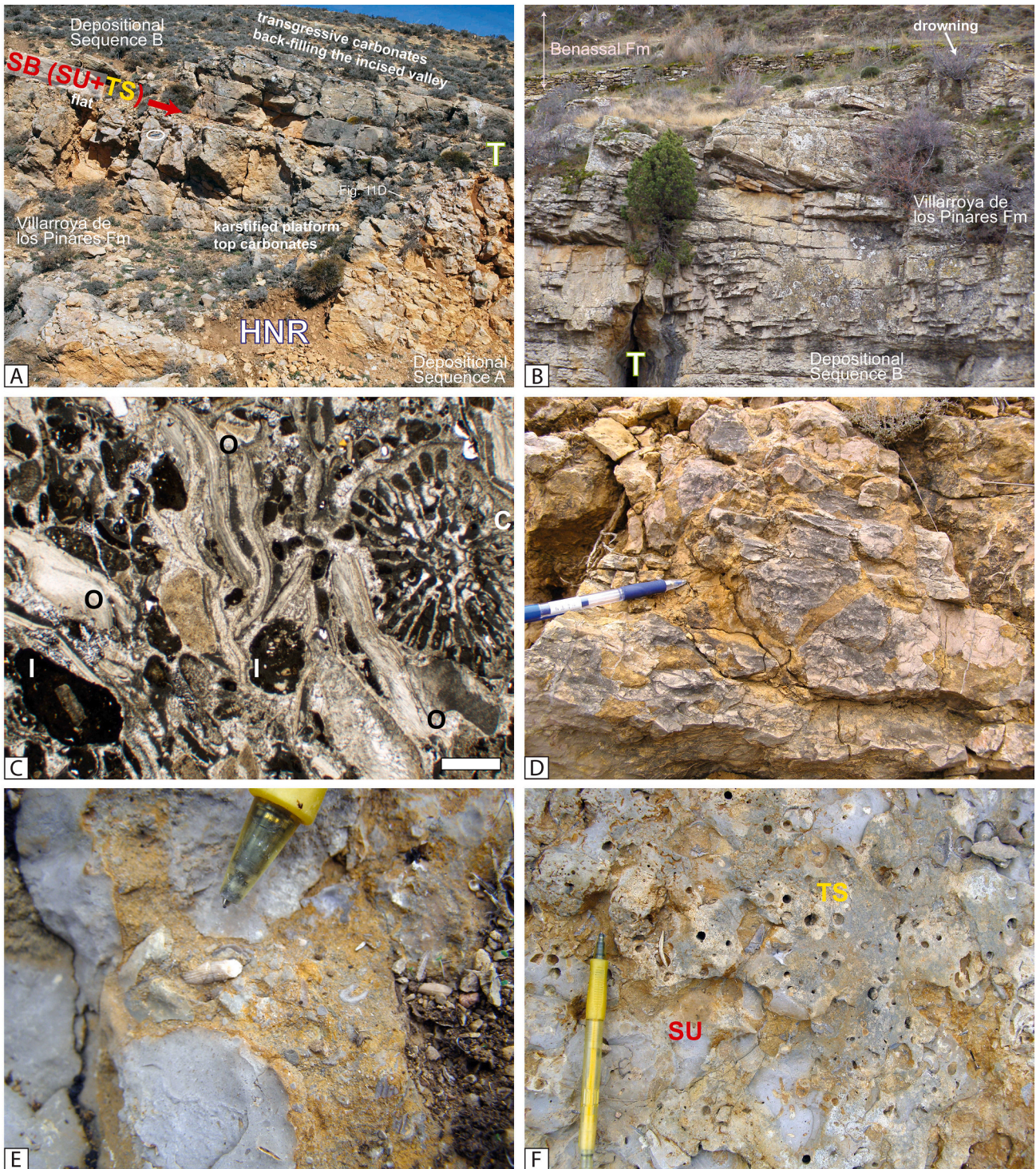


Fig. 11. Barranco de la Canal, Campillo Bajo and Camino de Camarillas. A) View and interpretation of the Camino de Camarillas outcrop including the composite sequence boundary (SU + TS), which separates subaerially exposed highstand platform carbonates below from transgressive strata above. In this outcrop, the subaerial unconformity exhibits a flat erosional profile. Encircled ruler = 15 cm. See Figs. 3 and 1C for key and location, respectively. B) Outcrop view and interpretation of the uppermost Villarroya de los Pinares Formation made up of transgressive grainstones exhibiting cross-bedding with local herring-bone structures. Note the drowning surface at the top of these higher-energy carbonates. Campillo Bajo. See Fig. 10B for location. See Fig. 3 for key. C) Photomicrograph of a grainstone texture rich in oysters (O), which is the most representative microfacies of the transgressive higher-energy unit of Depositional Sequence B. Note also the presence of intraclasts (I) and of a section of coral (C). Barranco de la Canal. See Fig. 9B for location. Scale = 1 mm. D) Close-up view of palaeokarst features found at the top of highstand normal regressive carbonates of the Villarroya de los Pinares Formation. Camino de Camarillas. See Fig. 11A for location. Visible part of pencil = 12 cm. E) Detail of the palaeokarst infilling, which locally includes coarse fragments of echinoid spines and bivalve shells. Campillo Bajo. Visible part of pencil = 2.5 cm. F) Close-up view of the composite sequence boundary showing the subaerial unconformity (SU) with palaeokarst features and the superposed transgressive surface (TS), which corresponds to a rockground exhibiting *Gastrochaenolites*. Campillo Bajo. See Fig. 3 for key. Pencil = 15 cm.

4.1.2.2. Palaeoenvironmental and sequence-stratigraphic interpretation. Aggrading inner parts of the highstand platform described at Las Mingachas crop out in the area of Camarillas (Figs. 1C and 3C). As a result of sea-level fall, these more proximal highstand limestones with rudists and corals were subaerially exposed and deeply incised (Figs. 9–10). The incision with an erosional relief of up to around 50 m and a width of up to 1.5 km, can be interpreted as a palaeo-valley. This unconformity surface with palaeokarst features (Figs. 11D-F) corresponds to a sequence boundary and separates Depositional Sequence A from Depositional Sequence B (Figs. 3C and 9-11A). The erosional surface incised in bedrock exhibits a characteristic stepped-like profile, with ramps and flats (Figs. 9-11A) corresponding to strath terraces, and resulting from alternating periods of stream-cutting erosion and lateral planation. In the proximal platform area of Camarillas, where accommodation apparently was reduced during deposition, lower-rank emersion surfaces related to higher-order sea-level events were also recorded within Depositional Sequence A (Bover-Arnal et al., 2009; see Fig. 9 in Gili et al., 2016).

During subsequent sea-level rise, the irregular topography created was flooded. Karst was filled with marine sediments (Figs. 11D-E) and the rockground substrate was extensively bored by lithophagid bivalves. The bedrock was also locally mineralized by iron oxides. Hence, the rockground corresponds to a transgressive surface that was superposed onto the subaerial unconformity giving rise to a composite sequence boundary (Figs. 3 and 9-11A). During the early transgression, oyster-bearing cross-bedded grainstones back-filled the incision created (Bover-Arnal et al., 2009, 2011). The back-filling strata commonly show yellow and orange colours that contrast with the gray colours marking the incised highstand normal regressive platform carbonates (Figs. 9–10).

The lower part of the palaeovalley infilling interpreted as early transgressive could have also been deposited during the lowstand normal regressive stage of relative sea level characterized at Las Mingachas (Fig. 3). However, stratal terminations and stacking patterns indicative of sedimentation during a specific relative sea-level stage are not present in these back-filling deposits. This is probably due to the limited depositional space within the narrow and long incised valleys. In this regard, incised valley-fill successions interpreted as transgressive deposits are common (e.g., Dalrymple et al., 1992; Chaumillon et al., 2008); also in Early Cretaceous examples (e.g., Ardies et al., 2002; Zaitlin et al., 2002; Raven et al., 2010).

In the course of transgression, the carbonate factory supplying sediment for these high-energy back-filling deposits became drowned (Figs. 9-10A-B and 11B). Drowning is marked by a hardground with iron-oxide mineralizations located at the top of the early transgressive oyster-bearing grainstones. This drowning surface was buried by late transgressive marls of the base of the Benassal Formation (Figs. 9 and 10A-B). Above the transgressive marls, platform carbonates of the Benassal Formation with rudists, corals and nerineid gastropods, correspond to highstand normal regressive deposits of Depositional Sequence B (Fig. 9).

4.2. Early late Aptian case study

4.2.1. Loma de Camarillas

In this subsection, the lower upper Aptian succession of the Loma de Camarillas site (Figs. 1C and 12) is analyzed for the first time. The succession belongs to the lower part of the Benassal Formation and includes a major erosional surface (sequence boundary), which separates depositional sequences B and C (Fig. 2). This section was logged (Fig. 13), sampled and described with focus on the sequence-stratigraphic interpretation and the characterization of the erosional surface (Fig. 14).

4.2.1.1. Description of the sedimentary succession. In the Loma de

Camarillas section, upper lower Aptian aggrading limestones rich in rudists of the Villarroya de los Pinares Formation are overlain by a 9 m-thick marl interval of terminal early and earliest late Aptian age belonging to the Benassal Formation (Figs. 12A-B and 13). The marls are characterized by the presence of large gastropods and levels with scleractinian corals in growth position. From metre 9.5 to metre 20.5 (Fig. 13), the succession is constituted by aggrading lower upper Aptian limestones with rudstone and floatstone textures dominated by rudists, but also including benthic foraminifera, fragments of echinoids and other molluscs. Above metre 20.5 and until metre 37.5 highly bioturbated nodular grey limestones rich in *Permocalculus* debris occur (Figs. 12–13). Besides *Permocalculus*, these bioturbated platform top carbonates also contain peloids, *Mesorbitolina texana* (Fig. 14A), miliolids, other benthic foraminifera, serpulids, gastropods, oysters and fragments of corals, rudists, other molluscs, echinoids and crinoids (Fig. 13).

At metre 37.5 (Fig. 13), a subaerial unconformity with a local down-cutting of c. 1 m into the lower upper Aptian aggrading *Permocalculus*-rich packstones of the lower Benassal Formation occurs (Figs. 12C-D and 14B-F). This erosional surface exhibits a flat-ramp geometry (Fig. 14B), and palaeokarst features with a depth penetration of up to c. 9 cm that are infilled with orangish carbonate (Figs. 14C-D). The palaeokarst-infilling carbonate and the succession overlying the subaerial unconformity from metre 37.5 to 42 are characterized by orangish limestones with grainstone and packstone textures mainly made up of crinoid and *Permocalculus* debris (Fig. 13). Other common to rare skeletal components identified in this latter stratigraphic interval include miliolids, other benthic foraminifera, gastropods, oysters, serpulids, and fragments of other molluscs, crustaceans, bryozoans, corals and echinoids. Non-skeletal grains include peloids, mud pebbles and drapes (Figs. 14C-E), quartz grains, and other lithoclasts (Fig. 14E), which exhibit the same facies as the underlying subaerially exposed greyish bioturbated packstones rich in *Permocalculus*. From metre 37.5 to 42 (Fig. 13), the strata are cross-bedded (Figs. 12C-D, 13 and 14F), include ripple marks, and locally show mm- to cm-thick laminations (Figs. 14C-E). At metre 42, the succession is cut by a thrust fault. Above, the underlying succession of platform carbonates with rudists and bioturbated *Permocalculus*-rich limestones is repeated and capped by a subaerial unconformity, which is overlain by Miocene conglomerates.

4.2.1.2. Palaeoenvironmental and sequence-stratigraphic interpretation.

The Loma de Camarillas section (Fig. 1C) starts with the more proximal parts of the highstand carbonate system of Depositional Sequence A. At this site, the Villarroya de los Pinares limestones are stacked in an aggrading pattern (Figs. 12A-B). These upper lower Aptian aggrading limestones with rudists and corals terminate with an incised subaerial unconformity; this is clearly shown in the vicinity of the town of Camarillas (Figs. 1C and 9–10), and in La Serna, to the east of the town of Jorcas, in the western limb of the Camarillas syncline (Fig. 1C; see Bover-Arnal et al., 2015).

With the subsequent transgressive event of Depositional Sequence B (Figs. 2, 12A-B and 13), a transgressive surface was superposed onto the subaerial unconformity. During the transgression, terminal lower and lower upper Aptian marls (lower part of the Benassal Formation) were deposited. The entire corals in life position recognized within the marl interval are indicative of slopes and distal platform environments (Bover-Arnal et al., 2012). The maximum flooding surface of Depositional Sequence B is traced along the top of this marl interval coinciding with the first downlap surface of platform carbonates with rudists (Figs. 12A-B and 13). The rudist-bearing strata and the above aggrading bioturbated limestones dominated by *Permocalculus* debris are interpreted as a highstand normal regressive succession (Figs. 12–13). As a result of sea-level fall during the uppermost *Epicheloniceras martini* ammonoid biozone (Fig. 2; see Bover-Arnal et al., 2016), these highstand platform carbonates, which are also part of the Benassal

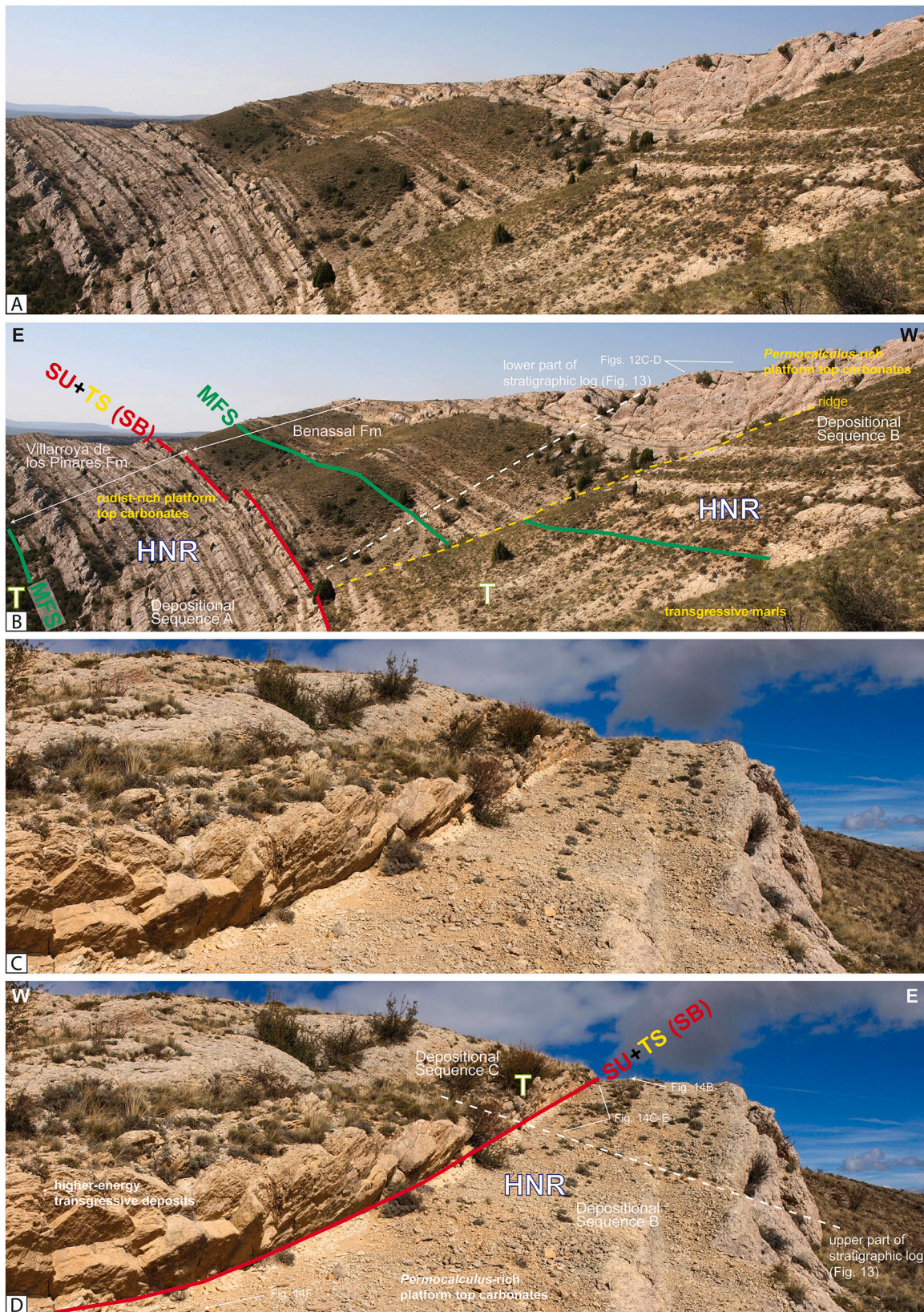


Fig. 12. Loma de Camarillas. A) Panoramic view of the lower part of the succession studied. B) Interpretation of Fig. 12A including the lithostratigraphic units, the sequence-stratigraphic framework, and the location of Figs. 12C-D and the lower part of the stratigraphic log shown in Fig. 13. Width of image = c. 200 m. C) Panoramic view of the upper part of the succession studied, which belongs to the Benassal Formation. D) Interpretation of Fig. 12C including the sequence-stratigraphic framework, and the location of Figs. 14B-F and the upper part of the stratigraphic log shown in Fig. 13. Width of image = c. 60 m. See Fig. 3 for key.

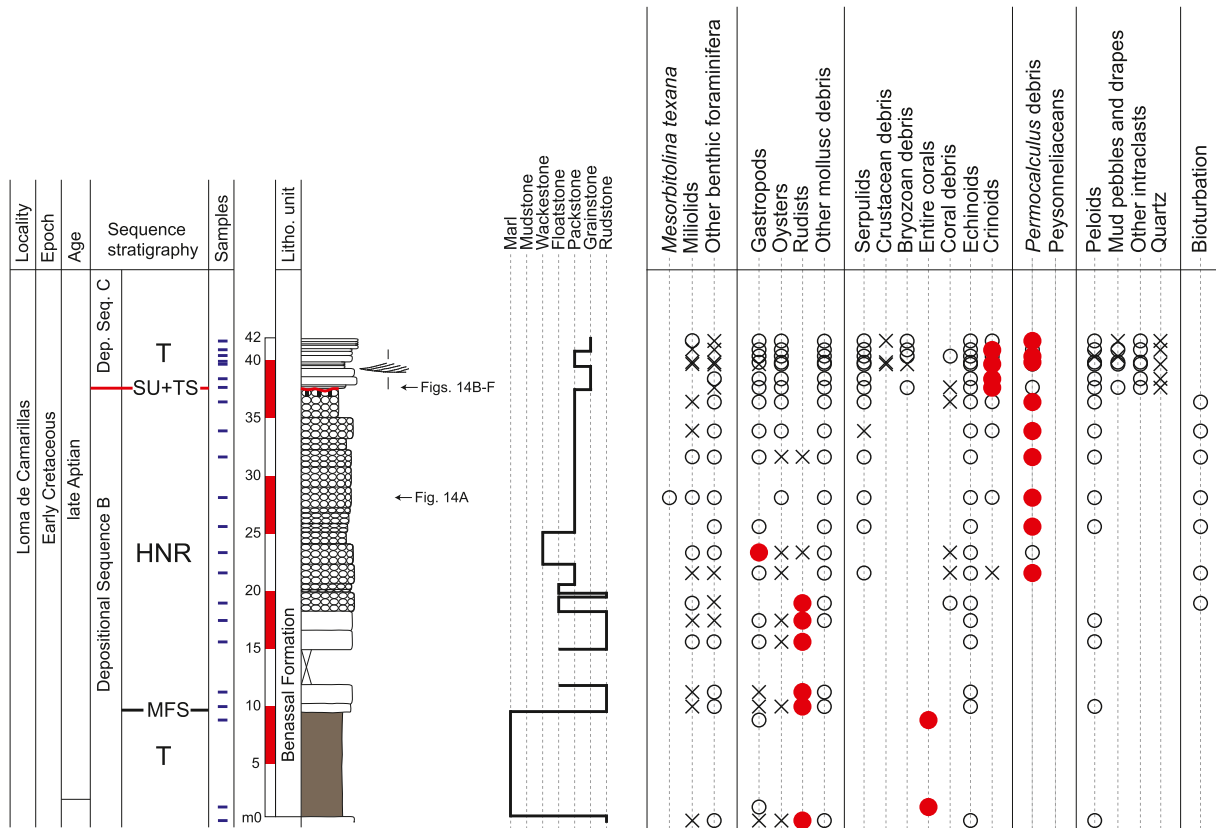


Fig. 13. Sedimentary log of the lower upper Aptian succession of Loma de Camarillas including depositional sequences B and C. The stratigraphic section displays the sequence-stratigraphic analysis, the stratigraphic position of the samples collected, the lithostratigraphic units, the lithologies, the bedding, the textures, the sedimentary features, the location of *figs. 14A-F*, and the stratigraphic position of the skeletal and non-skeletal components identified. See *Fig. 12* for location of the section. See *Figs. 3–4* for key.

Formation, were subaerially exposed, eroded and karstified (*Figs. 12C-D, 13 and 14B-F*).

During the subsequent transgression of Depositional Sequence C, packstone and grainstone carbonates infilled palaeokarst hollows (*Figs. 14C-D*), overlapped the ramps and covered the flats of the erosional surface carved into the underlying highstand normal regressive *Permocalculus*-rich packstones of Depositional Sequence C (*Fig. 14B*). The earliest transgressive deposits (Benassal Formation) resemble microbial mats developed in tidal coastal settings given that they are laminated to thinly-bedded (*Figs. 14C-E*) and show ripple marks (*Fig. 14E*) and mud pebbles and drapes (*Figs. 14C-E*). Such sedimentary features are known from modern tidal environments (e.g., *Franks and Stolz, 2009; Stal, 2012; Semeniuk, 2018*). Furthermore, the basal laminated succession includes intraclasts that were eroded from the underlying highstand succession and resedimented within the earliest transgressive deposits (*Fig. 14E*). The overlying packstone and grainstone orangish limestones rich in crinoid and *Permocalculus* debris exhibiting cross-bedding (*Figs. 13 and 14F*) indicate the establishment of higher-energy conditions during later stages of early transgression.

4.3. Amplitude of the Aptian relative sea-level fluctuations

The amplitude of the late early and early late Aptian major sea-level fluctuations can be estimated by measuring the depths of the incisions visible in the field (*Figs. 9–10, 14B and 15*). The incised erosional profiles formed during the late early Aptian sea-level drop in the Galve Sub-basin show maximum depths of around 15 m in the Campillo Bajo (*Figs. 1C and 10A-B*), and between 50 and 60 m in the Barranco de la Canal (*Figs. 1C and 9*; see also *Peropadre et al., 2013*). In the nearby La Serna creek (*Fig. 1C*), still within the Galve Sub-basin, *Bover-Arnal et al.*

(2015) reported a late early Aptian incision depth of up to 21 m. Taking the maximum depth measured on these incisions as an estimation, the amplitude of the late early Aptian sea-level fall in the Maestrat Basin was of around 50–60 m.

The lower upper Aptian sedimentary succession which recorded a major relative sea-level fall and rise analyzed in the Loma de Camarillas (*Fig. 1C*) does not show a deeply incised erosional profile. Incised valleys are local features, and in thrustured and eroded ancient successions the chances to find them exposed in outcrop are low. The lower upper Aptian subaerial unconformity investigated is slightly incised and cuts down into highstand platform carbonates of the Benassal Formation by as much as 1 m (*Fig. 14B*). This irregular surface exhibits palaeokarst features and is overlain by high-energy tidally-influenced carbonates (*Figs. 12C-D and 14B-F*).

The lower upper Aptian incised valley present in La Mola d'en Camaràs (*Fig. 15*) in the Morella Sub-basin (*Fig. 1B*) is the best preserved in the Maestrat Basin. *Bover-Arnal et al. (2014)* measured a minimum depth of 115 m for this incision (*Fig. 15*). However, considering the Neogene to present-day erosion of La Mola d'en Camaràs, the depth of the incised valley could have been ≥ 140 m (*Bover-Arnal et al., 2014*). Therefore, the amplitude of the major early late Aptian sea-level drop identified in the Maestrat Basin was in the order of 115 to 140 m, at least.

Major relative sea-level falls, surfaces of subaerial exposure and/or erosion, or significant sedimentary gaps were not identified in the Aptian valley-fill successions studied. The sedimentary infills described mainly show tidally-influenced grainstone deposits (*Figs. 9–10 and 11A-C*). These early transgressive higher-energy deposits are commonly capped by a hardground and buried by late transgressive marls (*Figs. 9, 10A-B and 11B*). Thus, the Aptian incised valleys were completely back-

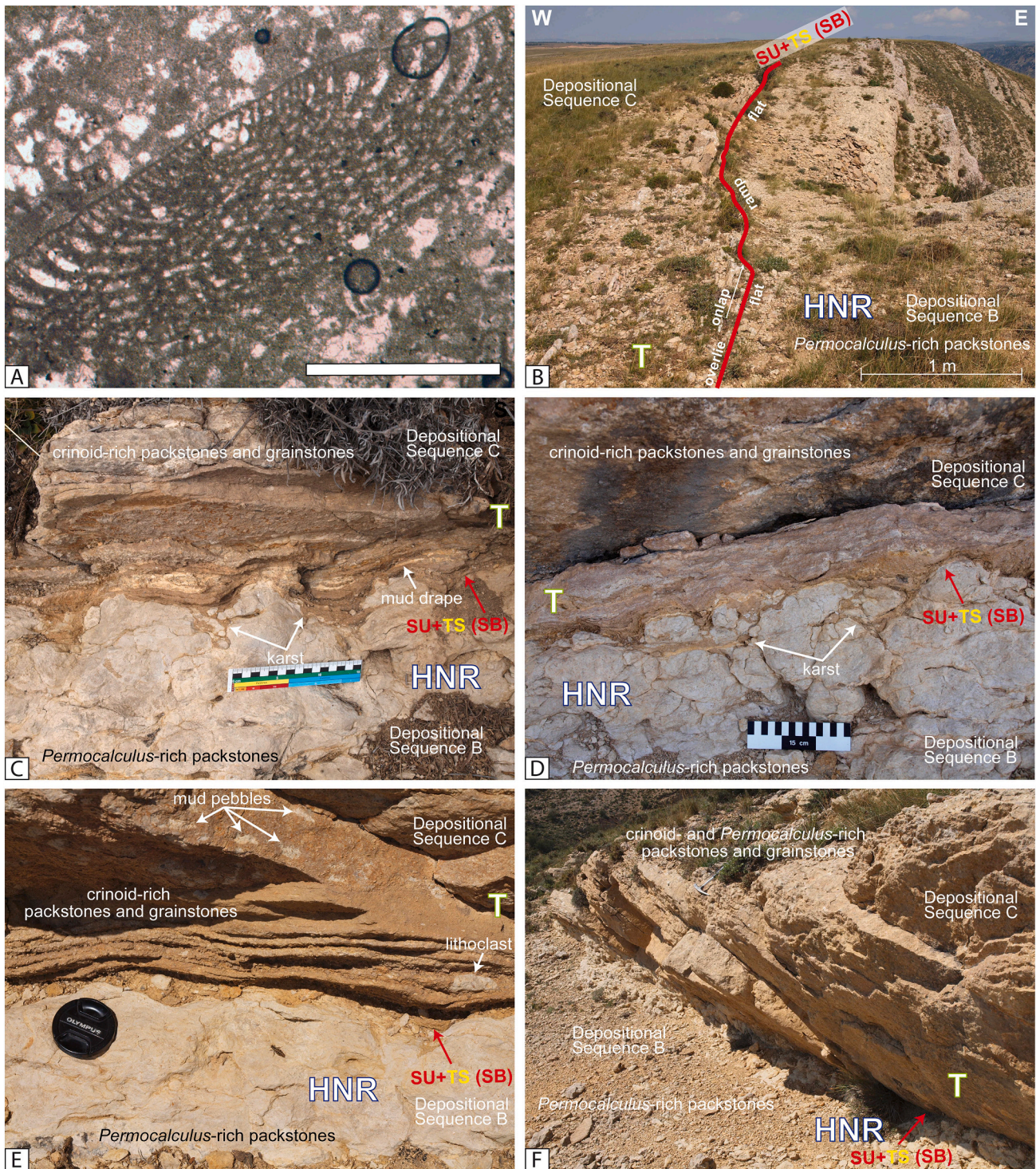


Fig. 14. Loma de Camarillas. A) Photomicrograph of a specimen of *Mesorbitolina texana* showing the embryonic apparatus. Highstand normal regressive platform carbonates of the Benassal Formation (early late Aptian). Depositional Sequence B. Scale = 1 mm. See Fig. 13 for location. B) Panoramic view of the lower upper Aptian erosional subaerial unconformity incised into the highstand normal regressive platform top carbonates of the Benassal Formation. Note how the transgressive surface is superposed onto the subaerial unconformity giving rise to a composite sequence boundary. This surface limits depositional sequences B and C. See Fig. 3 for key and Figs. 12D and 13 for location. C) Close-up view of the sequence boundary between depositional sequences B and C exhibiting palaeokarst features, which are found at the top of highstand normal regressive carbonates of the Benassal Formation. Note that the karst penetration depth is around 7 cm and how the sequence boundary corresponds to an irregular erosional surface. Note also the presence of mud drapes. See Fig. 3 for key and Figs. 12D and 13 for location. D) Detail of the erosional subaerial unconformity exhibiting infilled palaeokarst features, which show a depth penetration of c. 9 cm. Note the presence of thin mud drapes. See Fig. 3 for key and Figs. 12D and 13 for location. E) Close-up view of the irregular subaerial unconformity overlain by thinly bedded strata belonging to transgressive deposits of Depositional Sequence C. Note the presence of mud pebbles and of a lithoclast made up of highstand normal regressive platform top carbonates of Depositional Sequence B. Inset, and camera cap (= 5.8 cm) for scale. See Fig. 3 for key and Figs. 12D and 13 for location. F) Outcrop view of the composite sequence boundary between the highstand platform top carbonates rich in *Permocalculus* and the higher-energy cross-bedded transgressive packstones and grainstones containing abundant crinoid and *Permocalculus* debris. Hammer = 32 cm. See Fig. 3 for key and Figs. 12D and 13 for location.

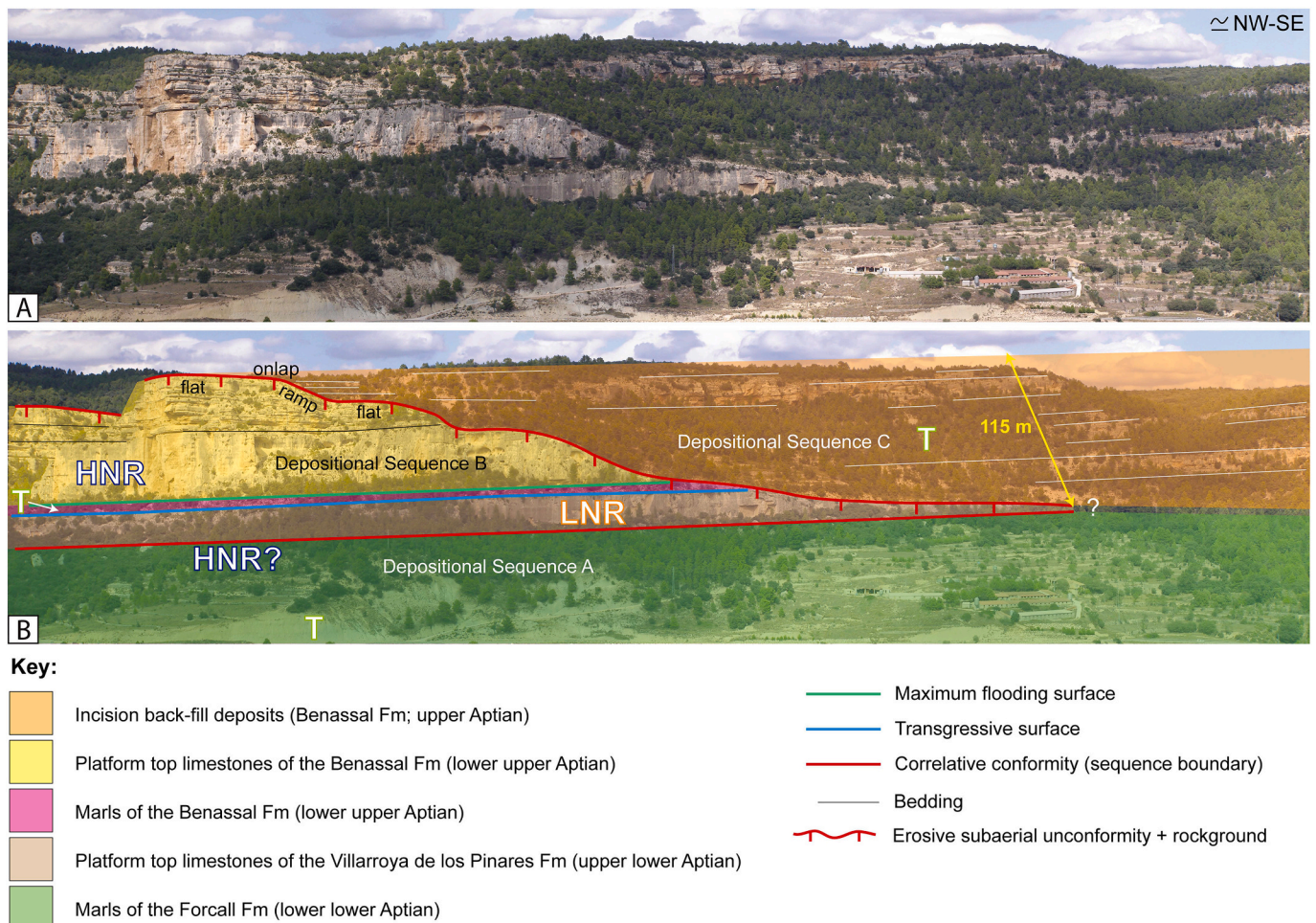


Fig. 15. La Mola d'en Camaràs. A) Panoramic view of the lower upper Aptian unconformity cropping out in the south-western face of the La Mola d'en Camaràs in the Morella Sub-basin (see Bover-Arnal et al., 2014). B) Sequence-stratigraphic interpretation of Fig. 15A. Note the stepped nature of the deeply incised unconformity surface down-cutting at least 115 m into the underlying Aptian record. See also key in Fig. 3.

filled during subsequent early transgression by marine deposits corresponding to a single depositional sequence (=simple fill *sensu* Zaitlin et al., 1994). Accordingly, the amplitudes of relative sea-level rise succeeding the late early and early late Aptian relative sea-level drops would have been of similar magnitude to those estimated for each major fall in relative sea level, i.e., 50–60 m and 115–140 m, respectively.

4.4. Assessment of the forced regressive wedge of Las Mingachas outcrop

Bover-Arnal et al. (2009) estimated a late early Aptian sea-level drop of c. 60 m at the platform margin of Las Mingachas by measuring the topographic difference between the top of the preserved preceding highstand platform carbonates (c. 1362 m; Fig. 6A) and the top of the forced regressive wedge of Depositional Sequence A (c. 1302 m; Figs. 3 and 5A-B). This amplitude of sea-level drop is in line with that obtained by measuring the depth of the upper lower Aptian incised valley present in the Barranco de la Canal (i.e., 50–60 m; Figs. 1C and 9).

The upper lower Aptian forced regressive grainstone wedge cropping out in Las Mingachas shows conspicuous sedimentological differences compared to the early transgressive grainstone deposits of late early Aptian age filling in incised valleys. The forced regressive basin floor component has a local significance, and does not crop out outside of Las Mingachas area, and has a lateral extension of <500 m (Fig. 3A-B). The early transgressive grainstone deposits, however, can be traced laterally for over one kilometre (Figs. 9 and 10). The forced regressive grainstone (Depositional Sequence A) containing *Permocalculus* and *Orbitolinopsis*

exhibits faint low-angle cross-bedding and overlies a sharp surface capping deeper-water basinal marly deposits (Figs. 3–5). The base and lower part of this grainstone succession is highly bioturbated and lacks mud pebbles and/or mud drapes (Figs. 4 and 5). On the other hand, the early transgressive grainstone deposits (Depositional Sequence B) covered erosional and irregular surfaces (Figs. 9 and 10), and bioturbation features are not prominent. They do exhibit tidal bundles, bidirectional sedimentary structures (Fig. 11B) and well-marked unidirectional cross-bedding. The lower part of these transgressive grainstone units frequently shows mud pebbles and drapes, which are indicative of erosion and reworking of lime mud deposited on the rockground during earliest transgression. Locally, these transgressive high-energy deposits also display conglomerate deposits.

Another difference between the forced regressive and transgressive grainstone units recognized in this study is that the transgressive grainstone deposits are not overlain by rudist- and coral-dominated carbonate platforms. They are topped by a hardground surface (see Fig. 14D in Bover-Arnal et al., 2015) and buried by late transgressive marls (Figs. 9, 10A-B and 11B). In contrast, the upper lower Aptian grainstone units interpreted as forced regressive successions in Las Mingachas (Figs. 3 and 5A-B) and also in the Mola de la Garumba (Morella Sub-basin; Fig. 1B; see Bover-Arnal et al., 2014) are down-lapped by lowstand platforms containing rudists and corals.

Forced regressive strata associated with the late early Aptian sea-level fall have only been identified in the platform to slope to basin transition area of Las Mingachas (Figs. 3–5) and in the Morella Sub-basin

(Bover-Arnal et al., 2014). The outcrop of Las Mingachas is unique while it shows two platform margins, one of a highstand platform (Fig. 6A) and a second one of lowstand platform (Fig. 6B). Both are very well-preserved and exposed in a small area of only 0.15 km² (Figs. 3A-B). Of significance is also that the Aptian sedimentary record of Las Mingachas can be studied in three dimensions exhibiting striking stacking patterns and stratal terminations (Figs. 3A-B and 6), which are commonly only recognizable on seismic lines.

4.5. Differing sequence-stratigraphic interpretations of Las Mingachas outcrop

In a different interpretation, Peropadre et al. (2013) reported up to six different regional composite scour surfaces (sequence boundaries) related to subaerial erosion for the upper lower Aptian succession of the Galve Sub-basin. The incised subaerial unconformity documented by Bover-Arnal et al. (2009) that separates depositional sequences A and B in the area of Camarillas (Figs. 1C and 9–10) corresponds to the regional composite scour surface VI of Peropadre et al. (2013). Peropadre et al. (2013) interpret this surface to truncate the carbonates of the Villarroya de los Pinares Formation in Las Mingachas outcrop as well. In contrast, Bover-Arnal et al. (2009) correlates the subaerial unconformity capping highstand platform top carbonates of Depositional Sequence A with a correlative conformity located at the top of a forced regressive wedge in Las Mingachas area (Fig. 3). In Las Mingachas outcrop, Peropadre et al. (2013; Fig. 7 therein) arranged the succession into a transgressive and two consecutive regressive systems tracts. These authors included the stratigraphic unit interpreted as a forced regressive wedge by Bover-Arnal et al. (2009, 2010, 2011) into their transgressive systems tract II.

Following Peropadre et al. (2013), Pomar and Haq (2016) questioned the late early Aptian sea-level fall recorded as a basin floor component in Las Mingachas and interpreted this grainstone wedge as a transgressive deposit. Pomar and Haq (2016) seek to refute the sub-basin scale sequence-stratigraphic framework discussed extensively by Bover-Arnal et al. (2009) but so merely by studying a stratigraphic interval with an extent of only 5 m in width and 15 m in thickness, which are approximated values, as their Fig. 25 lacks a precise scale. Although the rocks should be the same, the biotic content and its stratigraphic distribution, as well as some lithologies for this stratigraphic interval reported in their review are not in agreement with our observations (Fig. 16; compare also Fig. 25 in Pomar and Haq, 2016 with the present paper's subsection 4.1.1.1.). Besides, Pomar and Haq (2016) mis-correlate stratigraphic surfaces as their 'M' surface does not correlate with our basal surface of forced regression (Fig. 16; compare also Fig. 25 in Pomar and Haq, 2016 with Figs. 10–11 in Bover-Arnal et al., 2009 and Figs. 4–5 in this paper). The base of the grainstone unit as mis-correlated by Pomar and Haq (2016) and referred as surface 'M' is c. 1.5 m above the basal surface of forced regression interpreted by Bover-Arnal et al. (2009).

Finally, Pomar and Haq (2016) re-interpret the transition from the basin marls of the Forcall Formation (see Figs. 3-6A and 7A), which are dominated by large-sized discoidal *P. lenticularis* (Figs. 7C-D), to the grainstone wedge rich in *Permocalculus*, lumps of *M. lugeoni* and small-sized conical *Orbitolinopsis* (Figs. 8C-D; and not *Orbitolina* as Pomar and Haq, 2016 report) belonging to platform carbonates of the Villarroya de los Pinares Formation as a transgression. Pomar and Haq (2016) support this re-interpretation on the following rationale: "The grainstone unit 1) overlies marls with in-situ shallow water components, 2) it contains in its lower part reworked components from the underlying marls, and 3) these reworked shallow-water components disappear in the upper part". Each of the arguments is discussed below:

1) Pomar and Haq (2016) neither illustrate or precisely determine these "in-situ" shallow-water components nor provide a taphonomic analysis supporting their autochthonous nature. The uppermost part of the marls of the Forcall Formation underlying the grainstone unit in Las Mingachas (Fig. 5) contains skeletal grains characteristic of platform-top

settings such as rudists, corals and *Permocalculus* (Figs. 4 and 8A-B). However, these skeletal components are subordinate, and they appear as highly abraded and fragmented clasts (Figs. 8A-B) within marls and marly-limestones dominated by well-preserved tests of deeper-water biota such as large-sized discoidal *P. lenticularis* (see van Buchem et al., 2002) (Fig. 4). These marly deposits are laterally correlatable to topographically higher lying prograding carbonate slopes of a highstand platform (Fig. 3). Accordingly, the rudist, coral and *Permocalculus* debris are interpreted to have been shed from the platform top and transported downslope into the basin (see subsection 4.1.1.2.). Such re-sedimentation processes during highstand stages of sea level are widely known from ancient and modern carbonate platforms (e.g., Schlager et al., 1994; Everts et al., 1999; Reijmer et al., 2012, 2015).

2) Pomar and Haq (2016), again, do not document or show these reworked components from the underlying marls that they assert to be present in the grainstone unit. Moreover, they also do not report the biostratigraphic features they identified suggesting reworking of skeletal components from the underlying marls into the grainstone unit. The forced regressive wedge interpreted by Bover-Arnal et al. (2009) mainly exhibits packstone to grainstone textures (Fig. 4 and 8C-D). Hence, all the skeletal and non-skeletal components constituting these grain-supported textures are re-sedimented or reworked. In any case, the fact that the grainstone wedge could contain in its lower part reworked components from the underlying marls, is not incompatible with a higher-energy regressive nature of the deposit.

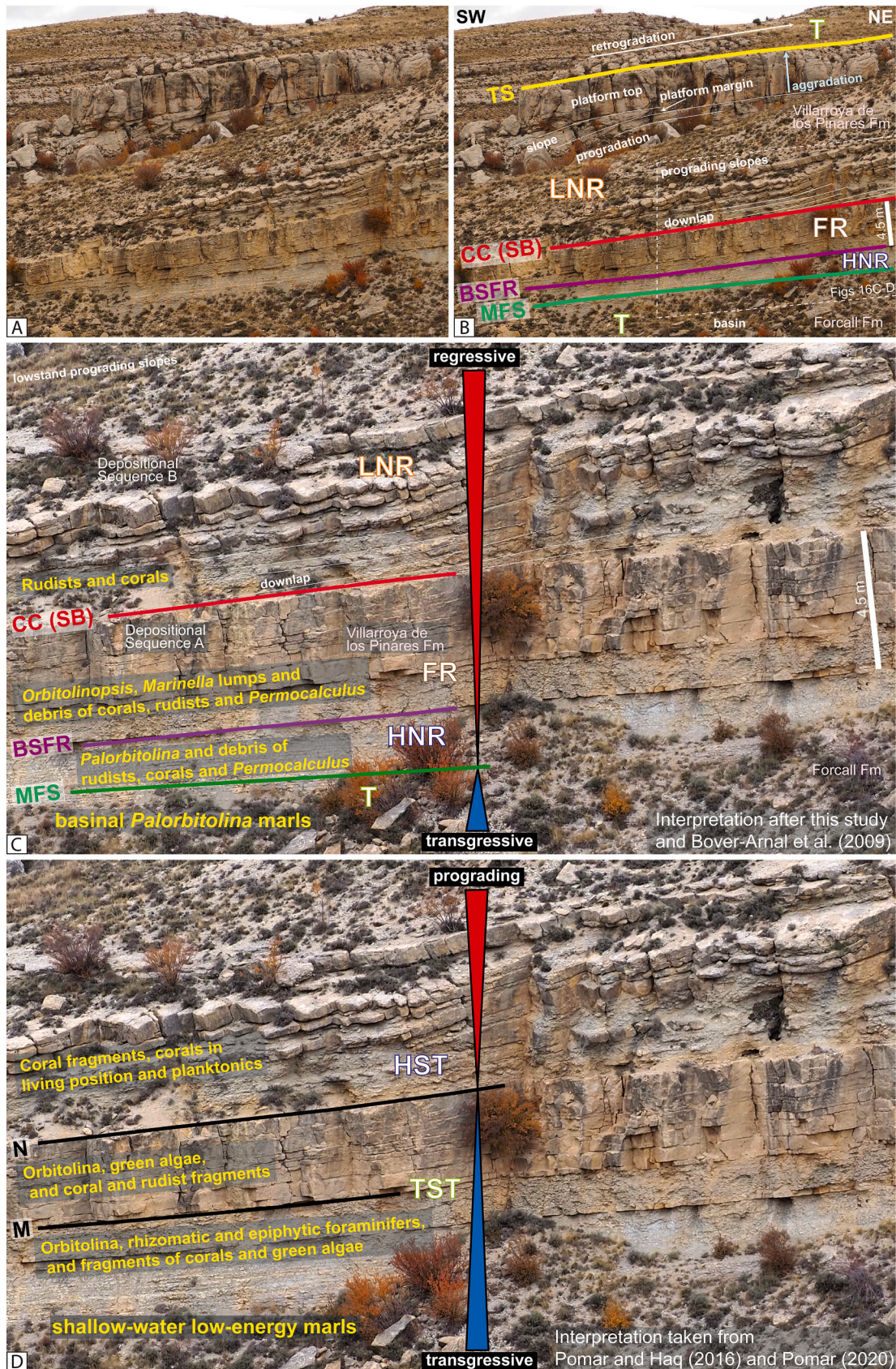
3) Throughout the grainstone wedge, shallower water components such as fragments of corals, *Permocalculus* and rudists not only do not disappear (Figs. 4 and 16) but dominate the facies together with other shallow-water skeletal grains such as *M. lugeoni* and *Orbitolinopsis* (Figs. 8C-D). The latter species do not occur below the basal surface of forced regression (Figs. 3–5 and 16). Therefore, and according to the results presented, no evidence of rising sea level occurs at the base of the grainstone wedge (BSFR in Figs. 3–5 and 16) but instead a change from a basinal deeper-water low-energy environment to shallower-water hydro-dynamically energetic conditions: a regression.

The interpretation of this upper lower Aptian grainstone wedge to represent a regression was again discussed as "erroneous" by Pomar (2020). Interestingly, the succession that Pomar (2020) interprets as a "highstand systems tract" is described and discussed by Bover-Arnal et al. (2009) as the lowstand carbonate platform downlapping over the forced regressive wedge (Fig. 16). This platform starts prograding, ends aggrading, and shows downlap stratal terminations (see Figs. 3 and 6B-D). All these features are in accordance with the current definition of a lowstand normal regression (e.g., Catuneanu et al., 2009).

In this publication we aim to provide (i) an interpretation that is based on a variety of original datasets collected from a large series of outcrops, and (ii) a sub-basin-wide characterization of this late early Aptian sea-level fall employing different scales of observation (see subsections 4.1.1.1. and 4.1.1.2.) to avoid misunderstanding, because a likely way to misinterpret geological outcrops is to take a look too closely from a single perspective. Based on all data an interpretation will be discussed, but the vast series of outcrop data and figures presented in this manuscript will allow for the reader to evaluate in detail the interpretations made and hence to agree or disagree with that presented here.

4.6. Duration of the Aptian relative sea-level fluctuations

The duration of the late early and early late Aptian major relative sea-level fluctuations is next estimated by means of published numerical ages and ammonoid biostratigraphy. *Dufrenoyia furcata* and *D. dufrenoyi* ammonoid specimens have been found in several depocentres of the Maestrat Basin, including the western limb of the Miravete anticline in the Galve Sub-basin (Fig. 1C; Bover-Arnal et al., 2010). They occur in the upper part of the basinal marls of the Forcall Formation and in the marly lowermost part of the Benassal Formation (Moreno-Bedmar et al., 2010,



(caption on next page)

Fig. 16. Differing interpretations of Las Mingachas outcrop. A) View of the sedimentary wedge interpreted as a forced regressive unit, which is underlain by highstand normal regressive and transgressive basinal marly deposits and overlain by the prograding slopes of a lowstand normal regressive platform. B) Interpretation of Fig. 16A including the lithostratigraphic units and the sequence-stratigraphic framework. The location of the photograph shown in Figs. 16C-D is indicated. See Fig. 3 for key and location. C) Close-up view of Fig. 16B showing the sequence-stratigraphic interpretation and the dominant skeletal components recognized in each genetic type of deposit. See Fig. 4 for a detailed description of the fossil content present in this stratigraphic interval. Note how the basal surface of forced regression corresponds to a sharp surface separating highstand basinal marls with *Palorbitolina* and debris of platform top biota (below) from a forced regressive thick marly-limestone and limestone unit (above) containing *Orbitolinopsis* and abundant lumps of *Marinella* and fragments of corals, rudists and *Permodaculus*. The nodular aspect of the lower part of this forced regressive wedge is due to intense bioturbation. The sequence boundary (correlative conformity) between depositional sequences A and B is interpreted to be located at the downlap surface of lowstand slope deposits onto the underlying higher-energy cross-bedded forced regressive unit. The interpretations are after this study and Bover-Arnal et al. (2009). See Fig. 3 for key. D) Interpretation of the same outcrop by Pomar and Haq (2016) and Pomar (2020). Note how the dominant biotic content they report for each interval, as well as their sequence-stratigraphic and environmental interpretations differ from the results presented in this paper and Bover-Arnal et al. (2009). Pomar and Haq (2016) and Pomar (2020) correlate the basal surface of forced regression of Bover-Arnal et al. (2009) to their 'M' surface. Note, however, that the basal surface of forced regression of Bover-Arnal et al. (2009) is a different surface, located c. 1.5 m below the 'M' surface of Pomar and Haq (2016) and Pomar (2020). TST = Transgressive Systems Tract. HST = Highstand Systems Tract.

2012; Bover-Arnal et al., 2010, 2014, 2016; Garcia et al., 2014). However, there are exceptions such as in the Oliete Sub-basin (Fig. 1B) where the Forcall Formation only recorded the uppermost part of the *Deshayesites forbesi* Zone (Moreno-Bedmar et al., 2010; Garcia et al., 2014), or the eastern limb of the Miravete anticline in the Galve Sub-basin (Fig. 1C), where the upper part of the Forcall Formation contains ammonites belonging to the *Deshayesites deshayesi* Zone (Bover-Arnal et al., 2010). Moreover, in Las Mingachas (Galve Sub-basin), *Dufrenoyia* ammonite specimens were collected within the forced regressive wedge of Depositional Sequence A and the slopes of the lowstand platform of Depositional Sequence B (Fig. 3; Bover-Arnal et al., 2009). *Dufrenoyia furcata* and *D. dufrenoyi* are index-species of the *D. furcata* biozone (e.g., Reboulet et al., 2018). According to the ammonite findings, the *D. furcata* Zone spans in the western limb of the Miravete anticline (Fig. 1C) the upper part of the Forcall Formation, the entire Villarroya de los Pinares Formation and the lowermost part of the Benassal Formation (Fig. 2). Hence, the major relative sea-level fluctuation recorded in the upper lower Aptian Villarroya de los Pinares Formation occurred within the *D. furcata* Zone (Fig. 2). In accordance with the numerical ages presented in Gradstein et al. (2004, 2012) and Ogg et al. (2016), this biozone had a duration of 0.9 My, whereas in a more recent version of the Geological Time Scale, Gale et al. (2020) give a duration of 0.4 My for this biozone. Therefore, the late early Aptian major fall and subsequent early rise of relative sea-level with an amplitude of around 50–60 m occurred in <0.9 My.

In the Maestrat Basin, *Epicheloniceras* ammonites occur in the marl interval of the lower, non-basal part of the Benassal Formation above the *D. dufrenoyi* occurrences (Moreno-Bedmar et al., 2010; Garcia et al., 2014; Bover-Arnal et al., 2016). This marly succession mainly corresponds to the transgressive stage of Depositional Sequence B (Fig. 2). On the other hand, specimens of *Parahoplites* occur in the second marl interval of the Benassal Formation corresponding to transgressive deposits of Depositional Sequence C. The latter marl unit overlies the regressive and early transgressive platform carbonates of the lower part of the Benassal Formation that recorded a major early late Aptian sea-level fall and rise (Fig. 2). These platform carbonates were deeply incised in the Morella Sub-basin (Figs. 1B and 15; see Bover-Arnal et al., 2014). A rudist shell collected in the upper part of the valley-fill succession of La Mola d'en Camaràs (Fig. 15) was dated by Bover-Arnal et al. (2016) using strontium-isotope stratigraphy based on McArthur et al. (2001) and Gradstein et al. (2004). The age interval obtained was 118.93 Ma (+0.73/−0.7), which correlates with the upper part of the *Epicheloniceras martini* and lowermost *Parahoplites melchioris* ammonoid biozones (Bover-Arnal et al., 2016). Therefore, the early late Aptian major sea-level drop and subsequent early rise recorded in the lower part of the Benassal Formation did occur within the upper *E. martini* Zone, perhaps also including the lowermost part of the *P. melchioris* Zone (Fig. 2). According to the ammonoid biostratigraphy tied to numerical ages in Gradstein et al. (2004), the *E. martini* ammonoid Zone had a duration of 3 My. In Gradstein et al. (2004) and Ogg et al. (2016), the

duration of this biozone is longer, 4.96 My. In Gale et al. (2020), the estimated duration of the *E. martini* Zone is much shorter, c. 1.2 My. Nevertheless, regardless of the version of the Geological Time Scale followed, the early late Aptian major sea-level fluctuation with an amplitude of ≥ 115 m occurred in the upper part of the *E. martini* Zone (Fig. 2), and thus its duration would have been <3 My.

4.7. Global significance of the Aptian relative sea-level fluctuations

Roughly coeval major relative sea-level falls and rises have been reported from other Aptian successions worldwide (Fig. 17; e.g., Röhl and Ogg, 1998; Gréselle and Pittet, 2005; Rameil et al., 2012; Maurer et al., 2010, 2013; Bover-Arnal et al., 2014, 2016; Horner et al., 2019; Ray et al., 2019; Simmons et al., 2020). Furthermore, the age and amplitude of the late early Aptian sea-level fall reported from eastern Iberia matches well with the global sea-level event KAp2 of Haq (2014). This sea-level event had a relative medium amplitude of 25–75 m and occurred around the early/late Aptian boundary (Haq, 2014). On the other hand, according to the ammonoid occurrences and age determinations based on strontium-isotope stratigraphy reported in the Maestrat Basin (Bover-Arnal et al., 2014, 2016), the early late Aptian sea-level drop studied shows a good correlation with the medium to major magnitude event KAp4 of Haq (2014). Therefore, only remarkable examples of Aptian major relative sea-level swings recorded in the Iberian, Arabian and Eurasian plates are next discussed.

In the North Cantabrian Basin (Iberian Plate), Schlagintweit et al. (2016) interpreted two transgressive-regressive sequences (II and III) of early and late Aptian age that match well with the chronology of depositional sequences A and B characterized herein (Fig. 2). Fernández-Mendiola et al. (2013), also in the Basque-Cantabrian Basin, documented the subaerial exposure of two consecutive upper lower Aptian highstand carbonate platforms belonging to the Zamaia Formation. The Zamaia Formation, which correlates with the upper *D. furcata* Zone, is overlain by lower upper Aptian transgressive marlstones of the Bilbao Formation (Fernández-Mendiola et al., 2013), and thus this sedimentary evolution and its timing shows remarkable similarities to the passage from the regressive and subaerially exposed platform carbonates of the Villarroya de los Pinares Formation to the transgressive marls of the lower part of the Benassal Formation in the Maestrat Basin (Fig. 2).

The evolution of the Aptian carbonate succession rich in rudists, corals, orbitolinids and *L. aggregatum* of the Shu'aiba Formation (eastern Arabian Plate; see e.g., Pittet et al., 2002; Hillgärtner et al., 2003; van Buchem et al., 2002, 2010; Yose et al., 2006; Maurer et al., 2010; Rameil et al., 2012), also shows striking similarities to that of the time-equivalent platforms of the Villarroya de los Pinares Formation of the Maestrat Basin (eastern Iberian Plate; Figs. 1B, 2 and 3). Upper lower-upper Aptian highstand platform carbonates of the Shu'aiba Formation were subaerially exposed because of major sea-level fall (van Buchem et al., 2010; Yose et al., 2010; Maurer et al., 2010, 2013). The estimated amplitude for this sea-level drop varies among the authors,

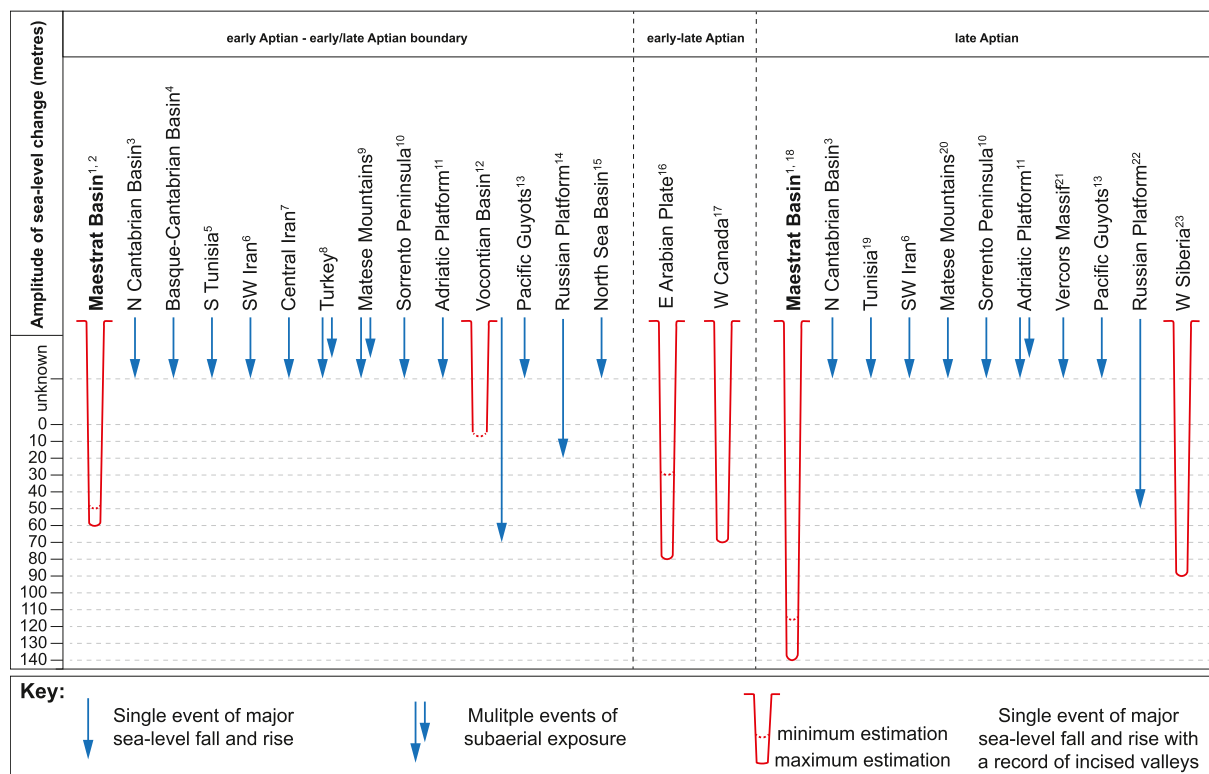


Fig. 17. Locations with geological evidence for major relative sea-level falls and rises during the early Aptian (including the early/late Aptian boundary) and the late Aptian. Where reported, estimates of the amplitude of sea-level change are indicated. The occurrence of roughly coeval Aptian major sea-level falls and rises in different tectonic plates, including the records of incised valleys in Iberia, Eurasia, Arabia and North America, is strong evidence for major eustatic fluctuations during the Aptian Stage. The data from the different locations are taken from ¹this study; ²Bover-Arnal et al. (2009, 2015, 2016); ³Schlagintweit et al. (2016); ⁴Fernández-Mendiola et al. (2013); ⁵Hfaiedh et al. (2013); ⁶Mehrabi et al. (2018); ⁷Wilmsen et al. (2015); ⁸Yilmaz and Altiner (2006); ⁹Ruberti et al. (2013); ¹⁰Graziano and Raspini (2015, 2018); ¹¹Husinec et al. (2012); ¹²Adatte et al. (2005) and Pictet et al. (2015); ¹³Röhl and Ogg (1998); ¹⁴Sahagian et al. (1996), Zorina and Ruban (2012) and Zorina (2014, 2016); ¹⁵van Buchem et al. (2018); ¹⁶van Buchem et al. (2002, 2010), Hillgärtner et al. (2003), Maurer et al. (2010, 2013), Raven et al. (2010), Yose et al. (2010) and Rameil et al. (2012); ¹⁷Horner et al. (2019); ¹⁸Bover-Arnal et al. (2014, 2016); ¹⁹Hfaiedh et al. (2013), Ben Chaabane et al. (2021); ²⁰Graziano et al. (2016); ²¹Adatte et al. (2005); ²²Sahagian et al. (1996); ²³Medvedev et al. (2011).

but ranges between 30 and 80 m (van Buchem et al., 2002; Hillgärtner et al., 2003; Maurer et al., 2010, 2013; Raven et al., 2010). Thus, the estimated amplitude for the late early Aptian relative sea-level fall in the Maestrat Basin (i.e., 50–60 m) agrees with those proposed for the eastern Arabian Plate. The subaerial exposure of the Shu'aiba Formation rocks started at the early/late Aptian boundary and reached into the late Aptian (van Buchem et al., 2010; Rameil et al., 2012; Maurer et al., 2013). On the contrary, in the Maestrat Basin, after a major fall in relative sea level in the late early Aptian (Figs. 9–10), a subsequent transgression commenced in the latest early Aptian, which was followed by a second major drop of early late Aptian age (Figs. 2, 12C-D, 13, 14B-F, 15 and 17; Bover-Arnal et al., 2014, 2016).

As described for the upper lower Aptian unconformity documented in the Maestrat Basin (Figs. 2, 9–10 and 11D-F), the top Shu'aiba unconformity shows palaeokarst features linked to subaerial exposure (Raven et al., 2010; Rameil et al., 2012). The latter surface is also superposed by iron oxide stains and lithophagid borings formed during the posterior earliest transgressive stage, and before the deposition of the overlying Nahr Umr Formation (Rameil et al., 2012).

On the Eurasian Plate, subaerial exposure surfaces capping upper lower Aptian platform carbonates were reported from southern Italy (Ruberti et al., 2013). These latter authors recognized up to ten different levels with palaeokarst filled with bauxite deposits within an upper lower-lower upper Aptian carbonate succession from the Matese Mountains. Still in the Matese Mountains, Graziano et al. (2016) studied a plant-rich Plattenkalk of early late Aptian age developed during a phase of long-lasting emersion that occurred in the uppermost *E. martini* biozone. Therefore, this phase of emersion was contemporaneous with

the lower upper Aptian major disconformity characterized in the Galve and Morella sub-basins (Figs. 2, 12C-D, 13, 14B-F, 15 and 17). At the Sorrento Peninsula (southern Italy), Graziano and Raspini (2015, 2018) analyzed a major erosional unconformity (disconformity) related with relative sea-level fall around the early/late Aptian boundary. Even more interestingly, Graziano and Raspini (2015, 2018) also identified and numerically dated a lower upper Aptian erosional surface truncating shallow-marine carbonates that is overlain by charophyte-rich limestones. This fall in sea-level was interpreted by Graziano and Raspini (2015, 2018) as triggered by glacio-eustasy and these authors provided a numerical age of 118.2 Ma for the erosional surface. This age is very similar to the numerical age of 118.93 Ma (+0.73/–0.7) obtained by Bover-Arnal et al. (2016) for the upper part of the preserved transgressive succession of Depositional Sequence C (Fig. 2), which back-fills the deeply incised unconformity cropping out in La Mola d'en Camaràs (Fig. 15) in the Morella Sub-basin (Fig. 1B).

A major loss of accommodation occurring during the late early Aptian was also recorded by Cretaceous carbonate platforms that flourished along the margin of the Vocontian Basin (e.g., Adatte et al., 2005; Pictet et al., 2015). This late early Aptian relative sea-level drop occurred within the *D. dufrenoyi* subzone (upper part of the *D. furcata* Zone) (e.g., Pictet et al., 2015), as recognized in the Maestrat Basin (Fig. 2). Associated with this fall in relative sea level is a major erosional, locally incised, unconformity (SbA3 in Adatte et al., 2005; D3 in Pictet et al., 2015). Pictet et al. (2015) measured a down-cutting of around 5 m in the Michelet section, whereas Adatte et al. (2005) gave an estimation of around 70 m for this late early Aptian relative sea-level fall. This latter magnitude of relative sea-level change is similar to the amplitude

estimated for the late early Aptian relative sea-level drop in the Maestrat Basin (i.e., 50–60 m; see Fig. 17). A second major fall in relative sea-level of early late Aptian age is recorded as a subaerial unconformity with palaeokarst development above in the succession in the Vercors Massif (Adatte et al., 2005) (Fig. 17).

4.8. Origin of the Aptian relative sea-level fluctuations

In all the incised erosional profiles described, the incised strata exhibit similar dips and dip directions to those of the deposits that back-filled the incision (Figs. 9–11A and 14B). Furthermore, in outcrops that were not significantly tilted, the apparent dip of the bedding of the incised bedrock and incision-fill succession is roughly horizontal (Fig. 10A–B). Another remarkable example of a rather tectonically undeformed incised valley exhibiting these characteristic sedimentary features is that of early late Aptian age found in La Mola d'en Camaràs in the Morella Sub-basin (Figs. 1B and 15; see Bover-Arnal et al., 2014). Therefore, the Aptian sedimentary record of relative sea-level oscillations do not show angular stratal relationships between the successions truncated and the overlying or infilling deposits (Figs. 9–11A, 14B and 15). This suggests the absence of tectonic tilting of the sedimentary succession during the Aptian sea-level changes identified.

The thicknesses of the Aptian successions recorded in the Maestrat Basin range from few metres (e.g., Salas, 1987) to >1300 m (e.g., Yao et al., 2020). With such variable and thick sedimentary records, it is evident that synrift subsidence played a role in controlling accommodation during the Aptian. Nevertheless, layers of rock uplifted 50–60 m without folding or tilting, exposed subaerially and incised, and then straightaway subsiding 50–60 m without folding or tilting while marine deposition resumes, and these occurring in a period <0.9 My, seems implausible. Therefore, according to the magnitude and global significance of the relative sea-level swings documented, the Aptian deeply incised unconformities and transgressive valley fills characterized are interpreted as resulting mainly from eustasy-driven sea-level fluctuations.

Ray et al. (2019) provided a synthesis of published estimations of magnitudes of relative sea-level change recorded during the Cretaceous in several basins worldwide. In this review, they noted that the amplitudes of relative sea-level change reported for the Aptian were significantly larger than those documented for older stages such as the Hauterivian and Barremian. The Hauterivian-Barremian major relative sea-level fluctuations typically reflect amplitudes between 30 and 40 m, whereas during Aptian times amplitudes of up to 60 m, with occasional larger events, were attained (Ray et al., 2019). These results fit well with the amplitude estimations measured in the Aptian record studied. In addition, Ray et al. (2019) also discussed the widespread development of deeply incised erosional profiles occurred during the Aptian, as shown in this paper (Figs. 9–10 and 15). Finally, Ray et al. (2019) concluded that Aptian amplitudes of relative sea-level change of >40 m likely resulted from glacio-eustasy. In fact, the amplitude and duration of the late early Aptian relative sea-level swing characterized in the Maestrat Basin, 50–60 m in <0.9 My, falls within the field of glacio-eustasy, i.e., tens of metres in <1 My (e.g., Immenhauser, 2005; Miller et al., 2005; Ray et al., 2019).

The late Pleistocene ice age resulted in a c. 120 m global sea-level drop (e.g., Fairbanks, 1989; Voris, 2000) during the marine isotope stage 2 (MIS 2; e.g., Lisiecki and Raymo, 2005). That required an expansion of continental ice in the northern hemisphere equivalent to covering half of North America and significant parts of Europe and Asia (e.g., Batchelor et al., 2019). Therefore, the interpreted relative sea-level excursion of 50 to 60 m in these (Figs. 3 and 9–10) and other late early Aptian sections worldwide would require a continental ice covering about half of that area. Regarding the sea-level fall of c. 115 m amplitude interpreted in the early late Aptian record of the Maestrat Basin (Fig. 15), the required volume of continental ice sheets should have been around late Pleistocene scales. Such significant glaciations should then

have produced major glacial till, loess silt, glacial-marine sediments and scouring into the ice-covered regions (see e.g., Domack, 1983; Brugger, 2006; Quirk et al., 2022).

Heimhofer et al. (2008), Rameil et al. (2012), Maurer et al. (2013), Horner et al. (2019) and Ray et al. (2019) show global palaeogeographic reconstructions compiling locations with reported evidence of Aptian relative sea-level drops and/or cool episodes, which would lend support to the view that active glacio-eustasy sea-level variations marked the late early-early late Aptian interval. Geochemical and sedimentological data such as lithology and colour of rocks, carbon and oxygen isotopes, sea-surface temperatures derived from TEX86 palaeothermometry, fluid inclusions, as well as reports of biotic (i.e., calcareous nannofossils, benthic and planktonic foraminifera, rudist bivalves, continental flora) changes found in the literature evidence the existence within the Cretaceous 'greenhouse', especially during the Aptian Stage, of relatively cool episodes (e.g., Weissert and Lini, 1991; Solé de Porta and Salas, 1994; Kemper, 1995; Hochuli et al., 1999; Herrle and Mutterlose, 2003; Pucéat et al., 2003; Weissert and Erba, 2004; Steuber et al., 2005; Ando et al., 2008; Heimhofer et al., 2008; Mutterlose et al., 2009; Skelton and Gili, 2012; McAnena et al., 2013; Millán et al., 2014; Bodin et al., 2015; Bottini et al., 2015; Cors et al., 2015; Bonin et al., 2016; Pascual-Cebrian et al., 2016; O'Brien et al., 2017; Zhang et al., 2017; Alley et al., 2019), which could have resulted in ice cap growth. In addition, numerical experiments based on palaeogeographic reconstructions and atmospheric CO₂ concentrations also support the transient formation of continental ice shields during the Cretaceous, more concretely, during the Aptian and the Maastrichtian stages (Ladant and Donnadieu, 2016).

Nevertheless, none of these studies unambiguously prove the growth and decay of significant ice sheets during the Aptian. In this regard, the occurrence of cool episodes or glaciations in the Cretaceous is still a matter of debate (e.g., Hay, 2016; Hay et al., 2019), as well as the glacial origin of dropstones, glendonites and deposits resembling tillites reported from Early Cretaceous successions (see e.g., Price, 1999; Teichert and Luppold, 2013; Morales et al., 2017; Hay et al., 2019; Tollefsen et al., 2020). Therefore, although the amplitudes and durations of relative sea-level change reported herein are in agreement with glacio-eustasy, the absence of an indisputable glacial sedimentary record of Early Cretaceous age, make of these Aptian major falls in relative sea level still largely a mystery.

5. Conclusions

The Aptian world recorded a strong eustatic signal. In the eastern margin of the Iberian Plate, eustasy-driven sea-level falls of late early and early late Aptian age were recorded either as forced regressive sedimentary wedges deposited at the toe of highstand slopes or as erosional surfaces cutting down highstand platform top carbonates. During subsequent sea-level rise, lowstand carbonate platforms developed above the forced regressive wedges and transgressive tidally-influenced deposits mainly back-filled the incised valleys created on the platform tops. In the Maestrat Basin and based on the depth of the erosional profiles identified, the late early and early late Aptian sea-level falls and rises analyzed had amplitudes of c. 50–60 m and ≥115 m, respectively. The late early Aptian fall and rise of sea level occurred within the *D. furcata* ammonite biozone, whereas the early late Aptian eustatic fluctuation took place around the transition between the *E. martini* and *P. melchioris* biozones. Accordingly, the durations for these major eustatic events were respectively <0.9 My and <3 My. The erosional profiles that resulted from the eustatic sea-level drop commonly show strath terraces. The incised highstand platform carbonates and their corresponding transgressive valley-fill deposits exhibit a similar dip and dip direction. In non-significantly structured outcrops, the bedding of the incised bedrock and back-filling peritidal strata is nearly horizontal. A non-angular stratal relationship above and below an incised subaerial unconformity (disconformity) is regarded as an

indicator for a major eustasy-driven fall and rise fluctuation of sea level in the rock record. Similar and coeval stratigraphic architectures of Aptian age were recorded along the margins of the Tethys and lend support to their eustatic origin. The interpreted amplitudes and durations of relative sea-level change fall within the glacio-eustatic domain. However, these would have been in need of important glaciations and development of continental ice sheets at least half as large as those developed during the last glaciation in the late Pleistocene. Nonetheless, undeniable sedimentary evidence of such significant growth of continental ice caps during the Aptian is lacking. Accordingly, the triggering of these Aptian variations in relative sea level is still not understood and perhaps was more likely not only the result of a single mechanism (i.e., glacio-eustasy) but presumably the fruit of several factors of relative sea-level change operating at different scales. Finally, the Aptian case studies presented herein constitute a reference for the interpretation and evaluation of such time-equivalent carbonate systems.

Declaration of Competing Interest

None.

Acknowledgements

We would like to express our deepest gratitude to John J.G. Reijmer for his support and for reviewing and greatly improving the first version of the manuscript. We thank the former Global and Planetary Change editor-in-chief and current associate editor Thomas M. Cronin for inviting us to write this contribution. Peter W. Skelton, Octavian Catuneanu, Antoine Pictet, Jean Borgomano, Stéphane Bodin, the current editor-in-chief Alan Haywood, the managing editor Howard Falcon-Lang and five anonymous reviewers provided helpful comments and corrections to earlier versions of the manuscript. We give them our most sincere thanks. This work is a contribution to IBERINSULA (PID2020-113912GB-I00) funded by MCIN/AEI/10.13039/501100011033 and the European Regional Development Fund (ERDF). Funding by the Grup de Recerca Reconegut per la Generalitat de Catalunya 2017 SGR 824 “Geologia Sedimentària” is acknowledged. Cristian Estop-Aragónés and Alia Ponz improved and sharpened the focus of parts of the text and figures. The drone aerial panorama shown in Fig. 9 was kindly provided by Riccardo Rocca. Felix Schlagintweit helped to identify several microfossils. Jordi Illa manufactured the thin sections used in this study. Marc Aurell and Álvaro García-Penas are thanked for fruitful discussions on the geology of the NW Maestrat Basin.

References

- Adatte, T., Arnaud Vanneau, A., Arnaud, H., 2005. The Hauterivian-lower Aptian sequence stratigraphy from Jura platform to Vocontian Basin: a multidisciplinary approach / Field-trip of the 7th International symposium on the Cretaceous (September 1-4, 2005); [organized by] Université Joseph Fournier, Grenoble 1 Université de Neuchâtel, UNINE. insu-00723810. <https://hal-insu.archives-ouvertes.fr/insu-00723810>.
- Al-Husseini, M.I., 2013. Antarctica's glacio-eustatic signature in the Aptian and late Miocene–Holocene: Implications for what drives sequence stratigraphy. *GeoArabia* 18, 17–52.
- Alley, N.F., Hore, S.B., Frakes, L.A., 2019. Glaciations at high-latitude Southern Australia during the Early Cretaceous. *Aust. J. Earth Sci.* <https://doi.org/10.1080/08120099.2019.1590457>.
- Álvarez, M., Capote, R., Vegas, R., 1979. Un Modelo de evolución geotectónica para la cadena Celtibérica. *Acta Geológica Hispánica* 14, 172–181.
- Ando, A., Kaiho, K., Kawahata, H., Kakegawa, T., 2008. Timing and magnitude of early Aptian extreme warming: unraveling primary $\delta^{18}O$ variation in indurated pelagic carbonates at Deep Sea Drilling Project Site 463, central Pacific Ocean. *Palaeogeogr. Palaeoclimatol. Palaeoecol.* 260, 463–476.
- Ardies, G.W., Dalrymple, R.W., Zaitlin, B.A., 2002. Controls on the geometry of incised valleys in the Basal Quartz Unit (Lower Cretaceous), Western Canada Sedimentary Basin. *J. Sediment. Res.* 72, 602–618.
- Batchelor, C.L., Margold, M., Krapp, M., Murton, D.K., Dalton, A.S., Gibbard, P.L., Stokes, C.R., Murton, J.B., Manica, A., 2019. The configuration of Northern Hemisphere ice sheets through the Quaternary. *Nat. Commun.* 10, 3713.
- Beavington-Penney, S.J., 2004. Analysis of the effects of abrasion on the test of *Palaeonummulites venosus*: implications for the origin of nummulithoclastic sediments. *Palaios* 19, 143–155.
- Ben Chaabane, N., Khemiri, F., Soussi, M., Belhaj Taher, I., 2021. Late Aptian carbonate platform evolution and controls (south Tethys, Tunisia): response to sea-level oscillations, palaeo-environmental changes and climate. *Facies* 67, 26.
- Bodin, S., Meissner, P., Janssen, N.M.M., Steuber, T., Mutterlose, J., 2015. Large igneous provinces and organic carbon burial: Controls on global temperature and continental weathering during the Early Cretaceous. *Glob. Planet. Chang.* 133, 238–253.
- Bonin, A., Pucéat, E., Vennin, E., Mattioli, E., Aurell, M., Joachimski, M., Barbarin, N., Laffont, R., 2016. Cool episode and platform demise in the Early Aptian: New insights on the links between climate and carbonate production. *Paleoceanography* 31, 66–80. <https://doi.org/10.1002/2015PA002835>.
- Bottini, C., Erba, E., Tiraboschi, D., Jenkyns, H.C., Schouten, S., Sinningh Damsté, J.S., 2015. Climate variability and ocean fertility during the Aptian Stage. *Clim. Past* 11, 383–402.
- Boudagher-Fadel, M.K., Price, G.D., 2019. Global evolution and paleogeographic distribution of mid-Cretaceous orbitolids. *UCL Open: Environment* 1, 01. <https://doi.org/10.14324/111.444/ucloe.000001>.
- Boullila, S., Galbrun, B., Miller, K.G., Pekar, S.F., Browning, J.V., Laskar, J., Wright, J.D., 2011. On the origin of Cenozoic and Mesozoic “third-order” eustatic sequences. *Earth Sci. Rev.* 109, 94–112.
- Bover-Arnal, T., Salas, R., Moreno-Bedmar, J.A., Bitzer, K., 2009. Sequence stratigraphy and architecture of a late Early-Middle Aptian carbonate platform succession from the western Maestrat Basin (Iberian Chain, Spain). *Sediment. Geol.* 219, 280–301.
- Bover-Arnal, T., Moreno-Bedmar, J.A., Salas, R., Skelton, P.W., Bitzer, K., Gili, E., 2010. Sedimentary evolution of an Aptian syn-rift carbonate system (Maestrat Basin, E Spain): effects of accommodation and environmental change. *Geol. Acta* 8, 249–280.
- Bover-Arnal, T., Salas, R., Skelton, P.W., Gili, E., Moreno-Bedmar, J.A., 2011. The Aptian carbonate platforms of the western Maestrat Basin: a textbook example of four systems tract-based sequence stratigraphy. In: Arenas, C., Pomar, L., Colombo, F. (Eds.), *Pre-meeting Field Trips Guidebook, 28th IAS Meeting, Zaragoza, Sociedad Geológica de España, Geo-Guías, vol. 7*, pp. 27–64.
- Bover-Arnal, T., Löser, H., Moreno-Bedmar, J.A., Salas, R., Strasser, A., 2012. Corals on the slope (Aptian, Maestrat Basin, Spain). *Cretac. Res.* 37, 43–64.
- Bover-Arnal, T., Salas, R., Guimerà, J., Moreno-Bedmar, J.A., 2014. Deep incision on an Aptian carbonate succession indicates major sea-level fall in the Cretaceous. *Sedimentology* 61, 1558–1593.
- Bover-Arnal, T., Pascual-Cebrian, E., Skelton, P.W., Gili, E., Salas, R., 2015. Patterns in the distribution of Aptian rudists and corals within a sequence-stratigraphic framework (Maestrat Basin, E Spain). *Sediment. Geol.* 321, 86–104.
- Bover-Arnal, T., Moreno-Bedmar, J.A., Frijia, G., Pascual-Cebrian, E., Salas, R., 2016. Chronostratigraphy of the Barremian-Early Albian of the Maestrat Basin (E Iberian Peninsula): integrating strontium-isotope stratigraphy and ammonoid biostratigraphy. *Newsl. Stratigr.* 49, 41–68.
- Brugger, K.A., 2006. Late Pleistocene climate inferred from the reconstruction of the Taylor River glacier complex, southern Sawatch Range, Colorado. *Geomorphology* 75, 318–329.
- Canérot, J., Crespo, A., Navarro, D., 1979. Montalbán, hoja n° 518. Mapa Geológico de España 1:50.000. 2ª Serie. 1ª Edición. Servicio de Publicaciones, Ministerio de Industria y Energía, Madrid, p. 31.
- Canérot, J., Cugny, P., Pardo, G., Salas, R., Villena, J., 1982. Ibérica Central-Maestrazgo. In: García, A. (Ed.), *El Cretácico de España*. Universidad Complutense de Madrid, pp. 273–344.
- Catuneanu, O., 2019. Model-independent sequence stratigraphy. *Earth Sci. Rev.* 188, 312–388.
- Catuneanu, O., Abreu, V., Bhattacharya, J.P., Blum, M.D., Dalrymple, R.W., Eriksson, P.G., Fielding, C.R., Fisher, W.L., Galloway, W.E., Gibling, M.R., Giles, K.A., Holbrook, J.M., Jordan, R., Kendall, C.G., Macurda, B., Martinsen, O.J., Miall, A.D., Neal, J.E., Nummedal, D., Pomar, L., Posamentier, H.W., Pratt, B.R., Sarg, J.F., Shanley, K.W., Steel, R.J., Strasser, A., Tucker, M.E., Winker, C., 2009. Towards the standardization of sequence stratigraphy. *Earth Sci. Rev.* 92, 1–33.
- Catuneanu, O., Galloway, W.E., Kendall, C.G., Miall, A.D., Posamentier, H.W., Strasser, A., Tucker, M.E., 2011. Sequence stratigraphy: methodology and nomenclature. *Newsl. Stratigr.* 44 (3), 173–245.
- Champetier, Y., Moullade, M., 1970. Correlations des facies a Orbitolinidae a l'Est du Rio Albaida, provinces de Valence et d'Alicante (Espagne); consequences stratigraphiques, paleoecologiques et paleogeographiques. *Bulletin de la Société Géologique de France S7-XII* (5), 765–773. <https://doi.org/10.2113/gssgbull.S7-XII.5.765>.
- Chaumillon, E., Proust, J.-N., Menier, D., Weber, N., 2008. Incised-valley morphologies and sedimentary-fills within the inner shelf of the Bay of Biscay (France): a synthesis. *J. Mar. Syst.* 72, 383–396.
- Christ, N., Immenhauser, A., Wood, R.A., Darwich, K., Niedermayr, A., 2015. Petrography and environmental controls on the formation of Phanerozoic marine carbonate hardgrounds. *Earth Sci. Rev.* 151, 176–226.
- Cloetingh, S., 1991. Tectonics and sea-level changes: a controversy? Ice age interludes during the time of Cretaceous greenhouse climate? In: Müller, D.W., McKenzie, J.A., Weissert, H. (Eds.), *Controversies in Modern Geology: Evolution of Geological Theories in Sedimentology*. Academic Press, Earth History and Tectonics, pp. 249–277.
- Cloetingh, S., Haq, B.U., 2015. Inherited landscapes and sea level change. *Science* 347. <https://doi.org/10.1126/science.1258375>.
- Conrad, C.P., 2013. The solid Earth's influence on sea level. *Geol. Soc. Am. Bull.* 125, 1027–1052.

- Cooper, M.R., 1977. Eustasy during the Cretaceous: its implications and importance. *Palaeogeogr. Palaeoclimatol. Palaeoecol.* 22, 1–60.
- Cors, J., Heimhofer, U., Adatte, T., Hochuli, P.A., Huck, S., Bover-Arnal, T., 2015. Spore-pollen assemblages show delayed terrestrial cooling in the aftermath of OAE 1a. *Geol. Mag.* 152, 632–647.
- Cronin, T.M., 1999. *Principles of Paleoclimatology*. Columbia University Press, New York, p. 560.
- Dalrymple, R.W., Zaitlin, B.A., Boyd, R., 1992. Estuarine facies models: Conceptual basis and stratigraphic implications. *J. Sediment. Petrol.* 62, 1130–1146.
- Davies, A., Gréselle, B., Hunter, S.J., Baines, G., Robson, C., Haywood, A.M., Ray, D.C., Simmons, M.D., van Buchem, F.S.P., 2020. Assessing the impact of aquifer-eustasy on short-term Cretaceous sea-level. *Cretac. Res.* 112, 104445.
- Domack, E.W., 1983. Facies of Late Pleistocene Glacial-Marine Sediments on Whidbey Island, Washington: An Isostatic Glacial-Marine Sequence. In: Molnia, B.F. (Ed.), *Glacial-Marine Sedimentation*. Springer, Boston, MA.
- Dunham, R.J., 1962. Classification of carbonate rocks according to depositional texture. In: Ham, W.E. (Ed.), *Classification of Carbonate Rocks*, American Association of Petroleum Geologists Memoire, vol. 1, pp. 108–121.
- Embry, A.F., Klovan, J.E., 1971. A Late Devonian reef tract on northeastern Banks Island, N.W.T. *Bull. Can. Petrol. Geol.* 19, 730–781.
- Embry, J.-C., Vennin, E., van Buchem, F.S.P., Schroeder, R., Pierre, C., Aurell, M., 2010. Sequence stratigraphy and carbon isotope stratigraphy of an Aptian mixed carbonate-siliciclastic platform to basin transition (Galve sub-basin, NE Spain). In: van Buchem, F.S.P., Gerdes, K.D., Esteban, M. (Eds.), *Mesozoic and Cenozoic Carbonate Systems of the Mediterranean and the Middle East: Stratigraphic and Diagenetic Reference Models*, vol. 329. Geological Society Special Publications, London, pp. 113–143.
- Everts, A.-J.W., Schlager, W., Reijmer, J.J.G., 1999. Carbonate platform-to-basin correlation by means of grain-composition logs: an example from the Vercors (Cretaceous, SE France). *Sedimentology* 46, 261–278.
- Fairbanks, R.G., 1989. A 17,000-year glacio-eustatic sea level record: influence of glacial melting rates on the Younger Dryas event and deep-ocean circulation. *Nature* 342, 637–642.
- Fernández-Mendiola, P.A., Mendicoa, J., Hernandez, S., Owen, H.G., García-Mondéjar, J., 2013. A facies model for an Early Aptian carbonate platform (Zamaia, Spain). *Facies* 59, 529–558.
- Franks, J., Stolz, J.F., 2009. Flat laminated microbial mat communities. *Earth-Science Reviews* 96, 163–172.
- Gale, A.S., Mutterlose, J., Batenburg, S., Gradstein, F.M., Agterberg, F.P., Ogg, J.G., Petrizzo, M.R., 2020. The cretaceous period. In: Gradstein, F.M., Ogg, J.G., Schmitz, M.D., Ogg, G.M. (Eds.), *Geologic Time Scale 2020*, volume 2. Elsevier, pp. 1023–1086.
- García, R., Moreno-Bedmar, J.A., Bover-Arnal, T., Company, M., Salas, R., Latil, J.L., Martín-Martín, J.D., Gomez-Rivas, E., Bulot, L.G., Delanoy, G., Martínez, R., Grauges, A., 2014. Lower Cretaceous (Hauterivian–Albian) ammonite biostratigraphy in the Maestrat Basin (E Spain). *J. Iber. Geol.* 40, 99–112.
- García-Senz, J., Salas, R., 2011. Sedimentary response to continental rifting in Iberia. In: Bádenas, B., Aurell, M., Alonso-Zarza, A.M. (Eds.), *Abstracts, 28th IAS Meeting of Sedimentology, Zaragoza, Spain*. IAS, p. 31.
- Gautier, F., 1980. Villarluengo, hoja n° 543. Mapa Geológico de España 1:50.000. 2ª Serie. 1ª Edición. Servicio de Publicaciones, Ministerio de Industria y Energía, Madrid, p. 45.
- Gili, E., Skelton, P.W., Bover-Arnal, T., Salas, R., Obrador, A., Fenerci-Masse, M., 2016. Depositional biofacies model for post-OAE1a Aptian carbonate platforms of the western Maestrat Basin (Iberian Chain, Spain). *Palaeogeogr. Palaeoclimatol. Palaeoecol.* 453, 101–114.
- Gradstein, F.M., Ogg, J.G., Smith, A.G., 2004. *A Geologic Time Scale 2004*. Cambridge University Press, Cambridge, p. 610.
- Gradstein, F.M., Ogg, J.G., Schmitz, M.D., Ogg, G.M., 2012. *The Geologic Time Scale 2012*. Elsevier. <https://doi.org/10.1016/C2011-1-08249-8>, 1176 pp.
- Granier, B., Dias-Brito, D., 2016. On the fossil alga *Marinella lugeoni* PFENDER, 1939, nom. cons., and its seven unfortunate avatars. Revision of the Juliette PFENDER Collection. Part 2 Revision of the Jesse Harlan JOHNSON Collection. Part 2. *Carnets Geol.* 16 (7), 231–245.
- Gratacós, Ó., Bover-Arnal, T., Clavera-Gispert, R., Carmona, A., García-Sellés, D., 2021. Forward numerical modelling constraining environmental parameters (Aptian carbonate system, E Iberia). *Mar. Pet. Geol.* 124, 104822.
- Graziano, R., Raspini, A., 2015. Long- and short-term hydroclimatic variabilities in the Aptian Tethys: clues from the orbital chronostratigraphy of evaporite-rich beds in the Apennine carbonate platform (Mt. Faito, southern Italy). *Palaeogeogr. Palaeoclimatol. Palaeoecol.* 418, 319–343.
- Graziano, R., Raspini, A., 2018. High-resolution chronostratigraphy of palaeoecologic and isotopic changes in shallow-marine carbonates: Deciphering the completeness of the Aptian record in the Apennine carbonate platform (southern Italy). *Cretac. Res.* 86, 97–128.
- Graziano, R., Raspini, A., Bartiromo, A., 2016. Late Aptian palaeoclimatic turnovers and volcanism: Insights from a shallow-marine and continental succession of the Apennine carbonate platform, southern Italy. *Sediment. Geol.* 339, 188–217.
- Gréselle, B., Pittet, B., 2005. Fringing carbonate platforms at the Arabian Plate margin in northern Oman during the Late Aptian–Middle Albian: Evidence for high-amplitude sea-level changes. *Sediment. Geol.* 175, 367–390.
- Gréselle, B., Pittet, B., 2010. Sea-level reconstructions from the Peri-Vocantian Zone (South-east France) point to Valanginian glacio-eustasy. *Sedimentology* 57, 1640–1684.
- Gronitz, V., 2017. Eustasy. In: Finkl, C.W., Makowski, C. (Eds.), *Encyclopedia of Coastal Science*. Springer International Publishing AG. https://doi.org/10.1007/978-3-319-48657-4_142-2.
- Guimerà, J., 1994. Cenozoic evolution of eastern Iberia: Structural data and dynamic model. *Acta Geol. Hisp.* 29, 57–66.
- Guimerà, J., 2018. Structure of an intraplate fold-and-thrust belt: The Iberian Chain. A synthesis. *Geol. Acta* 16, 427–438.
- Guimerà, J., Salas, R., 1996. Inversión terciaria de la falla normal mesozoica que limitaba la subcuena de Galve (cuena del Maestrazgo). *Geogaceta* 20, 1701–1703.
- Guimerà, J., Mas, R., Alonso, A., 2004. Intraplate deformation in the NW Iberian Chain: Mesozoic extension and Tertiary contractional inversion. *J. Geol. Soc. Lond.* 161, 291–303.
- Haq, B.U., 2014. Cretaceous eustasy revisited. *Glob. Planet. Chang.* 113, 44–58.
- Haq, B.U., Hardenbol, J., Vail, P.R., 1987. Chronology of fluctuating sea levels since the Triassic. *Science* 235, 1156–1167.
- Hardenbol, J., Thierry, J., Farley, M.B., Jacquin, T., Graciansky, De P.-C., Vail, P.R., 1998. Mesozoic and Cenozoic sequence stratigraphic framework of European basins. In: Graciansky, De P.-C., Hardenbol, J., Jacquin, T., Vail, P.R. (Eds.), *Mesozoic and Cenozoic sequence stratigraphy of European basins*, vol. 60. Society of Economic Paleontologists and Mineralogists Special Publication, pp. 3–13.
- Hay, W.W., 2016. Toward understanding Cretaceous climate—an updated review. *Sci. China Earth Sci.* 60, 5–19. <https://doi.org/10.1007/s11430-016-0095-9>.
- Hay, W.W., Leslie, M.A., 1990. Could possible changes in global ground-water reservoir cause eustatic sea-level fluctuations? In: Revelle, R. (Ed.), (Panel Chairman), *Sea-level change*. National Academy Press, Washington D.C., pp. 161–170.
- Hay, W.W., DeConto, R.M., de Boer, P., Flögel, S., Song, Y., Stepashko, A., 2019. Possible solutions to several enigmas of Cretaceous climate. *Int. J. Earth Sci.* <https://doi.org/10.1007/s00531-018-1670-2>.
- Heimhofer, U., Adatte, T., Hochuli, P.A., Burla, S., Weissert, H., 2008. Coastal sediments from the Algarve: low-latitude climate archive for the Aptian–Albian. *Int. J. Earth Sci.* 97, 785–797.
- Herrle, J.O., Mutterlose, J., 2003. Calcareous nannofossils from the Aptian–Lower Albian of southeast France: palaeoecological and biostratigraphic implications. *Cretac. Res.* 24, 1–22.
- Hfaiedh, R., Arnaud Vanneau, A., Godet, A., Arnaud, H., Zghal, I., Ouali, J., Latil, J.-L., Jallali, H., 2013. Biostratigraphy and palaeoenvironmental evolution of the Aptian succession at Jebel Bir Oum Ali (Northern Chain of Chotts, South Tunisia). *Cretac. Res.* 46, 177–207.
- Hillgärtner, H., Van Buchem, F.S.P., Gaumet, F., Razin, P., Pittet, B., Grötsch, J., Droste, H., 2003. The Barremian–Aptian evolution of the eastern Arabian carbonate platform margin (northern Oman). *J. Sediment. Res.* 73, 756–773.
- Hochuli, P.A., Menegatti, A.P., Weissert, H., Riva, A., Erba, E., Premoli Silva, I., 1999. Episodes of high productivity and cooling in the early Aptian Alpine Tethys. *Geology* 27, 657–660.
- Horner, S.C., Hubbard, S.M., Martin, H.K., Hagstrom, C.A., Leckie, D.A., 2019. The impact of Aptian glacio-eustasy on the stratigraphic architecture of the Athabasca Oil Sands, Alberta, Canada. *Sedimentology* 66, 1600–1642.
- Hunt, D., Tucker, M.E., 1992. Stranded parasequences and the forced regressive wedge systems tract: deposition during base-level fall. *Sediment. Geol.* 81, 1–9.
- Husinec, A., Harman, C.A., Regan, S.P., Mosher, D.A., Sweeney, R.J., Read, J.F., 2012. Sequence development influenced by intermittent cooling events in the Cretaceous Aptian greenhouse, Adriatic platform, Croatia. *AAPG Bull.* 96, 2215–2244.
- Immenhauser, A., 2005. High-rate sea-level change during the Mesozoic: New approaches to an old problem. *Sediment. Geol.* 175, 277–296.
- Kemper, E., 1995. The causes of the carbonate and colour changes in the Aptian of NW Germany. *Neues Jb. Geol. Paläontol. Abh.* 196, 275–289.
- Ladant, J.-P., Donnadieu, Y., 2016. Palaeogeographic regulation of glacial events during the Cretaceous supergreenhouse. *Nat. Commun.* 7, 12771. <https://doi.org/10.1038/ncomms12771>.
- Li, M., Hinnov, L.A., Huang, C., Ogg, J.G., 2018. Sedimentary noise and sea levels linked to land–ocean water exchange and obliquity forcing. *Nat. Commun.* 9, 1004.
- Liesa, C.L., Soria, A.R., Meléndez, N., Meléndez, A., 2006. Extensional fault control on the sedimentation patterns in a continental rift basin: El Castellar Formation, Galve sub-basin, Spain. *J. Geol. Soc. Lond.* 163, 487–498.
- Lisiecki, L.E., Raymo, M.E., 2005. A pliocene-pleistocene stack of 57 globally distributed benthic $\delta^{18}\text{O}$ records. *Paleoceanography* 20, PA1003.
- Martín-Chivelet, J., López-Gómez, J., Aguado, R., Arias, C., Arribas, J., Arribas, M.E., Aurell, M., Bádenas, B., Benito, M.I., Bover-Arnal, T., Casas-Sainz, A., Castro, J.M., Coruña, F., de Gea, G.A., Fornós, J.J., Fregenal-Martínez, M., García-Senz, J., Garófano, D., Gelabert, B., Giménez, J., González-Acebrón, J., Guimerà, J., Liesa, C. L., Mas, R., Meléndez, N., Molina, J.M., Muñoz, J.A., Navarrete, R., Nebot, M., Nieto, L.M., Omodeo-Salé, S., Pedrera, A., Peropadre, C., Quijada, I.E., Quijano, M.L., Reolid, M., Robador, A., Rodríguez-López, J.P., Rodríguez-Perea, A., Rosales, I., Ruiz-Ortiz, P.A., Sàbat, F., Salas, R., Soria, A.R., Suarez-Gonzalez, P., Vilas, L., 2019. The late Jurassic–early cretaceous rifting. In: Quesada, C., Oliveira, J.T. (Eds.), *The Geology of Iberia: A Geodynamic Approach. Volume 3: The Alpine Cycle*. Springer, Heidelberg, pp. 60–63. <https://doi.org/10.1007/978-3-030-11295-0>.
- Martín-Martín, J.D., Gomez-Rivas, E., Bover-Arnal, T., Travé, A., Salas, R., Moreno-Bedmar, J.A., Tomás, S., Corbella, M., Teixell, A., Vergés, J., Stafford, S.L., 2013. The Upper Aptian to Lower Albian synrift carbonate succession of the southern Maestrat Basin (Spain): Facies architecture and fault-controlled stratabound dolostones. *Cretac. Res.* 41, 217–236.
- Martín-Martín, J.D., Travé, A., Gomez-Rivas, E., Salas, R., Sizun, J.-P., Vergés, J., Corbella, M., Stafford, S.L., Alfonso, P., 2015. Fault-controlled and stratabound dolostones in the Late Aptian–earliest Albian Benassal Formation (Maestrat Basin, E Spain): Petrology and geochemistry constrains. *Mar. Pet. Geol.* 65, 83–102.

- Masse, J.-P., 2003. Integrated stratigraphy of the Lower Aptian and applications to carbonate platforms: a state of the art. In: Gili, E., Negra, H., Skelton, P.W. (Eds.), North African Cretaceous carbonate platform systems, NATO Science Series, IV. Earth and Environmental Sciences, vol. 28. Kluwer Academic Publishers, pp. 215–227.
- Matthews, R.K., Frohlich, C., 2002. Maximum flooding surfaces and sequence boundaries: comparisons between observations and orbital forcing in the Cretaceous and Jurassic (65–190 Ma). *GeoArabia* 7, 503–538.
- Maurer, F., Al-Mehsin, K., Pierson, B.J., Eberli, G.P., Warrlich, G., Drysdale, D., Droste, H.J., 2010. Facies characteristics and architecture of Upper Aptian Shu'aiba clinofolds in Abu Dhabi. In: van Buchem, F.S.P., Al-Husseini, M.I., Maurer, F., Droste, H.J. (Eds.), Barremian – Aptian Stratigraphy and Hydrocarbon Habitat of the Eastern Arabian Plate, vol. 2. *GeoArabia Special Publication* 4, Gulf PetroLink, Bahrain, pp. 445–468.
- Maurer, F., van Buchem, F.S.P., Eberli, G.P., Pierson, B.J., Raven, M.J., Larsen, P.-H., Al-Husseini, M.I., Vincent, B., 2013. Late Aptian long-lived glacio-eustatic lowstand recorded on the Arabian Plate. *Terra Nova* 25, 87–94.
- McAnena, A., Flögel, S., Hofmann, P., Herrle, J.O., Griesand, A., Pross, J., Talbot, H.M., Rethemeyer, J., Wallmann, K., Wagner, T., 2013. Atlantic cooling associated with a marine biotic crisis during the mid-Cretaceous period. *Nat. Geosci.* 6, 558–561.
- McArthur, J.M., Howarth, R.J., Bailey, T.R., 2001. Strontium isotope stratigraphy: lowess version 3. Best-fit to the marine Sr-isotope curve for 0 to 509 Ma and accompanying look-up table for deriving numerical age. *J. Geol.* 109, 155–170.
- Medvedev, A.L., Lopatin, A.Y., Masalkin, Y.V., 2011. Comparative characteristics of the lithological composition of the incised valley fill and host sediments of the Vikulovo Formation, Kamenny Area, West Siberia. *Lithol. Miner. Resour.* 46, 369–381.
- Mehrabi, H., Rahimpour-Bonab, H., Al-Aasm, I., Hajikazemi, E., Esrafil-Dizaji, B., Dalvand, M., Omidvar, M., 2018. Palaeo-exposure surfaces in the Aptian Dariyan Formation, offshore SW Iran: geochemistry and reservoir implications. *J. Pet. Geol.* 41, 467–494.
- Miall, A.D., 1997. *The Geology of Stratigraphic Sequences*. Springer-Verlag, Berlin, p. 433.
- Millán, M.I., Weissert, H.J., López-Horgue, M.A., 2014. Expression of the late Aptian cold snaps and the OAE1b in a highly subsiding carbonate platform (Aralar, northern Spain). *Palaeogeogr. Palaeoclimatol. Palaeoecol.* 411, 167–179.
- Miller, K.G., Komins, M.A., Browning, J.V., Wright, J.D., Mountain, G.S., Katz, M.E., Sugarman, P.J., Cramer, B.S., Christie-Blick, N., Pekar, S.F., 2005. The Phanerozoic record of global sea-level change. *Science* 310, 1293–1298.
- Morales, C., Rogov, M., Wierzbowski, H., Ershova, V., Suan, G., Adatte, T., Föllmi, K.B., Tegelaar, E., Reichart, G.-J., de Lange, G.J., Middelburg, J.J., van de Schootbrugge, B., 2017. Glendonites track methane seepage in Mesozoic polar seas. *Geology* 45, 503–506. <https://doi.org/10.1130/G38967.1>.
- Moreno-Bedmar, J.A., Company, M., Bover-Arnal, T., Salas, R., Maurrasse, F.J., Delanoy, G., Grauges, A., Martínez, R., 2010. Lower Aptian ammonite biostratigraphy in the Maestrat Basin (Eastern Iberian Chain, Eastern Spain). A Tethyan transgressive record enhanced by synrift subsidence. *Geol. Acta* 8, 281–299.
- Moreno-Bedmar, J.A., Bover-Arnal, T., Barragán, R., Salas, R., 2012. Uppermost Lower Aptian transgressive records in Mexico and Spain: chronostratigraphic implications for the Tethyan sequences. *Terra Nova* 24, 333–338.
- Mutterlose, J., Bornemann, A., Herrle, J., 2009. The Aptian–Albian cold snap: evidence for “mid” Cretaceous icehouse interludes. *N. Jb. Geol. Paläont. (Abh.)* 252, 217–225.
- Nebot, M., Guimerà, J., 2016. Structure of an inverted basin from subsurface and field data: the Late Jurassic–Early Cretaceous Maestrat Basin (Iberian Chain). *Geol. Acta* 14, 155–177.
- O'Brien, C.L., Robinson, S.A., Pancost, R.D., Sinninghe Damsté, J.S., Schouten, S., Lunt, D.J., Alsenz, H., Bornemann, A., Bottini, C., Brassell, S.C., Farnsworth, A., Forster, A., Huber, B.T., Inglis, G.N., Jenkyns, H.C., Linnert, C., Littler, K., Markwick, P., McAnena, A., Mutterlose, J., Naafs, B.D.A., Püttmann, W., Sluijs, A., van Helmond, N.A.G.M., Vellekoop, J., Wagner, T., Wrobel, N.E., 2017. Cretaceous sea-surface temperature evolution: Constraints from TEX 86 and planktonic foraminiferal oxygen isotopes. *Earth Sci. Rev.* 172, 224–247. <https://doi.org/10.1016/j.earscirev.2017.07.012>.
- Ogg, J.G., Ogg, G.M., Gradstein, F.M., 2016. *A Concise Geologic Time Scale 2016*. Elsevier. <https://doi.org/10.1016/C2009-0-64442-1>, 240 pp.
- Pascual-Cebrian, E., Götz, S., Bover-Arnal, T., Skelton, P.W., Gili, E., Salas, R., Stinnesbeck, W., 2016. Calcite/aragonite ratio fluctuations in Aptian rudist bivalves: Correlation with changing temperatures. *Geology* 44, 135–138.
- Peropadre, C., Liesa, C.L., Meléndez, N., 2013. High-frequency, moderate to high-amplitude sea-level oscillations during the late Early Aptian: insights into the mid-Aptian event (Galve sub-basin, Spain). *Sediment. Geol.* 294, 233–250.
- Pictet, A., Delanoy, G., Adatte, T., Spangenberg, J.E., Baudouin, C., Boselli, P., Boselli, M., Kindler, P., Föllmi, K.B., 2015. Three successive phases of platform demise during the early Aptian and their association with the oceanic anoxic Selli episode (Ardeche, France). *Palaeogeogr. Palaeoclimatol. Palaeoecol.* 418, 101–125.
- Pittet, B., van Buchem, F.S.P., Hillgärtner, H., Razin, P., Grötsch, J., Droste, H., 2002. Ecological succession, palaeoenvironmental change, and depositional sequences of Barremian–Aptian shallow-water carbonates in northern Oman. *Sedimentology* 49, 555–581.
- Pomar, L., 2020. Carbonate systems. In: Scarselli, N., Adam, J., Chiarella, D., Roberts, D. G., Bally, A.W. (Eds.), *Regional Geology and Tectonics. Volume 1: Principles of Geologic Analysis*. Elsevier, pp. 235–311.
- Pomar, L., Haq, B.U., 2016. Decoding depositional sequences in carbonate systems: Concepts vs experience. *Glob. Planet. Chang.* 146, 190–225.
- Price, G.D., 1999. The evidence and implications of polar ice during the Mesozoic. *Earth Sci. Rev.* 48, 183–210.
- Pucéat, E., Lécuyer, C., Sheppard, S.M.F., Dromart, G., Reboulet, S., Grandjean, P., 2003. Thermal evolution of Cretaceous Tethyan marine waters inferred from oxygen isotope composition of fish tooth enamels. *Palaeogeography* 18, PA1029.
- Quirk, B.J., Huss, E., Laabs, B.J.C., Leonard, E., Licciardi, J., Plummer, M.A., Caffee, M. W., 2022. Late Pleistocene glacial chronologies and paleoclimate in the northern Rocky Mountains. *Clim. Past* 18, 293–311.
- Rameil, N., Immenhauser, A., Csoma, A.E., Warrlich, G., 2012. Surfaces with a long history: the Aptian top Shu'aiba Formation unconformity, Sultanate of Oman. *Sedimentology* 59, 212–248.
- Raven, M.J., van Buchem, F.S.P., Larsen, P.-H., Surlyk, F., Steinhardt, H., Cross, D., Klem, N., Emang, M., 2010. Late Aptian incised valleys and siliciclastic infill at the top of the Shu'aiba Formation (Block 5, offshore Qatar). In: van Buchem, F.S.P., Al-Husseini, M.I., Maurer, F., Droste, H.J. (Eds.), Barremian – Aptian Stratigraphy and Hydrocarbon Habitat of the Eastern Arabian Plate, 2. *GeoArabia Special Publication* 4, Gulf PetroLink, Bahrain, pp. 469–502.
- Ray, D.C., van Buchem, F.S.P., Baines, G., Davies, A., Gréselle, B., Simmons, M.D., Robson, C., 2019. The magnitude and cause of short-term eustatic Cretaceous sea-level change: A synthesis. *Earth Sci. Rev.* 197, 102901.
- Reboulet, S., Szives, O., Aguirre-Urreta, B., Barragán, R., Company, M., Frau, C., Kakabadze, M.V., Klein, J., Moreno-Bedmar, J.A., Lukeneder, A., Pictet, A., Ploch, I., Raisosadat, S.N., Vascek, Z., Baraboshkin, E.J., Mitta, V.V., 2018. Report on the 6th International Meeting of the IUGS Lower Cretaceous Ammonite Working Group, the Kilian Group (Vienna, Austria, 20th August 2017). *Cretac. Res.* 91, 100–110.
- Reijmer, J.J.G., Palmieri, P., Groen, R., 2012. Compositional variations in calciturbidites and calcidibrites in response to sea-level fluctuations (Exuma Sound, Bahamas). *Facies* 58, 493–507.
- Reijmer, J.J.G., Palmieri, P., Groen, R., Floquet, M., 2015. Calciturbidites and calcidibrites: Sea-level variations or tectonic processes? *Sediment. Geol.* 317, 53–70.
- Röhl, U., Ogg, J.G., 1998. Aptian-albian eustatic sea-levels. In: Camoin, G.F., Davies, P.J. (Eds.), *Reefs and Carbonate Platforms in the Pacific and Indian Oceans*, vol. 25. International Association of Sedimentologists, Special Publications, pp. 93–136. <https://doi.org/10.1002/9781444304879.ch6>.
- Rovere, A., Stocchi, P., Vacchi, M., 2016. Eustatic and relative sea level changes. *Curr. Clim. Change Rep.* 2, 221–231.
- Ruberti, D., Bravi, S., Carannante, G., Vigorito, M., Simone, L., 2013. Decline and recovery of the Aptian carbonate factory in the southern Apennine carbonate shelves (southern Italy): Climatic/oceanographic vs. local tectonic controls. *Cretac. Res.* 39, 112–132.
- Sahagian, D., Pinous, O., Olfieriev, A., Zakharov, V., 1996. Eustatic curve for the Middle Jurassic–Cretaceous based on Russian Platform and Siberian stratigraphy: zonal resolution. *AAPG Bull.* 80, 1433–1458.
- Salas, R., 1987. *El Malm i el Cretaci inferior entre el Massís de Garraf i la Serra d'Espadà. Anàlisi de Conca*. PhD thesis. Universitat de Barcelona, 541 pp. <http://hdl.handle.net/10803/669675>.
- Salas, R., Casas, A., 1993. Mesozoic extensional tectonics, stratigraphy, and crustal evolution during the Alpine cycle of the eastern Iberian basin. *Tectonophysics* 228, 33–55.
- Salas, R., Guimerà, J., Mas, R., Martín-Closas, C., Meléndez, A., Alonso, A., 2001. Evolution of the Mesozoic Central Iberian Rift System and its Cainozoic inversion (Iberian Chain). In: Ziegler, P.A., Cavazza, W., Robertson, A.H.F., Crasquin-Soleau, S. (Eds.), *Peri-Tethys Memoir 6: Peri-Tethyan Rift/Wrench Basins and Passive Margins*, 186. Mémoires du Muséum National d'Histoire Naturelle, Paris, pp. 145–186.
- Salas, R., García-Senz, J., Guimerà, J., Bover-Arnal, T., 2010. Opening of the Atlantic and development of the Iberian intraplate rift basins during the late Jurassic–early Cretaceous. In: Pena Dos Reis, R., Pimentel, N. (Eds.), *II Central & north Atlantic Conjugate Margins Conference, Lisbon 2010. Rediscovering the Atlantic: New Ideas for an Old Sea. Extended Abstracts*, 3, pp. 245–248. ISBN: 978-989-96923-1-2.
- Sames, B., Wägrich, M., Wendler, J.E., Haq, B.U., Conrad, C.P., Melinte-Dobrinescu, M. C., Hu, X., Wendler, I., Wolfgring, E., Yilmaz, I.O., Zorina, S.O., 2016. Review: short-term sea-level changes in a greenhouse world – A view from the Cretaceous. *Palaeogeogr. Palaeoclimatol. Palaeoecol.* 441, 393–411.
- Sames, B., Wägrich, M., Conrad, C.P., Iqbal, S., 2020. Aquifer-eustasy as the main driver of short-term sea-level fluctuations during Cretaceous hothouse climate phases. In: Wägrich, M., Hart, M.B., Sames, B., Yilmaz, I.O. (Eds.), *Cretaceous Climate Events and Short-Term Sea-Level Changes*. Geological Society, London, p. 498. <https://doi.org/10.1144/SP498-2019-105>. Special Publications.
- Schlager, W., 1981. The paradox of drowned reefs and carbonate platforms. *Geol. Soc. Am. Bull.* 92, 197–211.
- Schlager, W., Reijmer, J.J.G., Droxler, A., 1994. Highstand shedding of carbonate platforms. *J. Sediment. Res.* 64, 270–281.
- Schlagintweit, F., Rosales, I., Najjarro, M., 2016. *Glomospirella cantabrica* n. sp., and other benthic foraminifera from Lower Cretaceous Urganion-type carbonates of Cantabria, Spain: biostratigraphic implications. *Geol. Acta* 14, 113–138.
- Semeniuk, V., 2018. *Encyclopedia of Coastal Science. Encyclopedia of Earth Sciences Series*. In: Finkl, C., Makowski, C. (Eds.). Springer, Cham, 10.1007/978-3-319-48657-4_317-2.
- Shinn, E.A., 1969. Submarine lithification of Holocene carbonate sediments in the Persian Gulf. *Sedimentology* 12, 109–144.
- Simmons, M.D., Miller, K.G., Ray, D.C., Davies, A., van Buchem, F.S.P., Gréselle, B., 2020. Phanerozoic Eustasy. In: Gradstein, F.M., Ogg, J.G., Schmitz, M.D., Ogg, G.M. (Eds.), *Geologic Time Scale 2020*, volume 1. Elsevier, pp. 357–400.
- Simón, J.L., Liesa, C.L., Soria, A.R., 1998. Un sistema de fallas normales sinesedimentarias en las unidades de facies Urgon de Aliaga. *Geogaceta* 24, 291–294.
- Skelton, P.W., Gili, E., 2012. Rudists and carbonate platforms in the Aptian: a case study on biotic interactions with ocean chemistry and climate. *Sedimentology* 59, 81–117.

- Skelton, P.W., Gili, E., Bover-Arnal, T., Salas, R., Moreno-Bedmar, J.A., 2010. A new species of *Polyconites* from the uppermost Lower Aptian of Iberia and the early evolution of polyconitid rudists. *Turk. J. Earth Sci.* 19, 557–572.
- Solé de Porta, N., Salas, R., 1994. Conjuntos microfiorísticos del Cretácico inferior de la Cuenca del Maestrazgo. Cordillera Ibérica Oriental (NE de España). *Cuadernos de Geología Ibérica* 18, 355–368.
- Stal, L.J., 2012. Cyanobacterial Mats and Stromatolites. In: Whitton, B.A. (Ed.), *Ecology of Cyanobacteria II: Their Diversity in Space and Time*, 65. Springer, pp. 65–125. https://doi.org/10.1007/978-94-007-3855-3_4.
- Steuber, T., Rauch, M., Masse, J.-P., Graaf, J., Malkoc, M., 2005. Low-latitude seasonality of Cretaceous temperatures in warm and cold episodes. *Nature* 437, 1341–1344.
- Stoll, H.M., Schrag, D.P., 1996. Evidence for glacial control of rapid sea level changes in the Early Cretaceous. *Science* 272, 1771–1774.
- Strasser, A., Hillgärtner, H., Hug, W., Pitter, B., 2000. Third-order depositional sequences reflecting Milankovitch cyclicity. *Terra Nova* 12, 303–311.
- Teichert, B.M.A., Luppold, F.W., 2013. Glendonites from an Early Jurassic methane seep—climate or methane indicators? *Palaeogeogr. Palaeoclimatol. Palaeoecol.* 390, 81–93.
- Tollefsen, E., Balic-Zunic, T., Mörth, C.-M., Brüchert, V., Lee, C.C., Skelton, A., 2020. Ikaite nucleation at 35°C challenges the use of glendonite as a paleotemperature indicator. *Sci. Rep.* 10, 8141.
- Vail, P.R., Audemard, F., Bowman, S.A., Eisner, P.N., Perez-Cruz, C., 1991. The stratigraphic signatures of tectonics, eustasy and sedimentology - an overview. In: Einsele, G., Ricken, W., Seilacher, A. (Eds.), *Cycles and Events in Stratigraphy*. Springer, Berlin, pp. 617–659.
- van Buchem, F.S.P., Pittet, B., Hillgärtner, H., Al Mansouri, A.I., Billing, I.M., Droste, H. H.J., Oterdoom, H., van Steenwinkel, M., 2002. High-resolution sequence stratigraphic architecture of Barremian/Aptian carbonate systems in Northern Oman and the United Arab Emirates (Kharaiib and Shu'aiba Formations). *GeoArabia* 7, 461–500.
- van Buchem, F.S.P., Al-Husseini, M.I., Maurer, F., Droste, H.J., Yose, L.A., 2010. Sequence-stratigraphic synthesis of the Barremian – Aptian of the eastern Arabian Plate and implications for the petroleum habitat. In: van Buchem, F.S.P., Al-Husseini, M.I., Maurer, F., Droste, H.J. (Eds.), *Barremian – Aptian Stratigraphy and Hydrocarbon Habitat of the Eastern Arabian Plate*, vol. 1. *GeoArabia Special Publication 4*, Gulf PetroLink, Bahrain, pp. 9–48.
- van Buchem, F.S.P., Smit, F.W.H., Buijs, G.J.A., Trudgill, B., Larsen, P.-H., 2018. Tectonostratigraphic framework and depositional history of the Cretaceous–Danian succession of the Danish Central Graben (North Sea) – new light on a mature area. *Geological Society, London, Petroleum Geology Conference Series* 8 (1), 9–46. <https://doi.org/10.1144/pgc8.24>.
- Vennin, E., Aurell, M., 2001. Stratigraphie séquentielle de l'Aptien du sous-basin de Galvé (Province de Teruel, NE de l'Espagne). *Bull. Soc. Geol. Fr.* 172 (4), 397–410.
- Vergés, J., Poprawski, Y., Almar, Y., Drzewiecki, P.A., Moragas, M., Bover-Arnal, T., Macchiavelli, C., Wright, W., Messenger, G., Embry, J.-C., Hunt, D., 2020. Tectono-sedimentary evolution of Jurassic–Cretaceous diapiric structures: Miravete anticline, Maestrat Basin, Spain. *Basin Res.* 32, 1653–1684.
- Voris, H.K., 2000. Maps of Pleistocene sea levels in Southeast Asia: shorelines, river systems and time durations. *J. Biogeogr.* 27, 1153–1167.
- Weisser, D., 1959. Acerca de la estratigrafía del Urgo-Aptense en las cadenas Celtibéricas de España. *Notas y comunicaciones del Instituto Geológico y Minero de España* 55, 17–32.
- Weissert, H., Erba, E., 2004. Volcanism, CO₂ and palaeoclimate: a Late Jurassic–Early Cretaceous carbon and oxygen isotope record. *J. Geol. Soc. Lond.* 161, 695–702.
- Weissert, H., Lini, A., 1991. Ice age interludes during the time of Cretaceous greenhouse climate? In: Müller, D.W., McKenzie, J.A., Weissert, H. (Eds.), *Controversies in Modern Geology: Evolution of Geological Theories in Sedimentology, Earth History and Tectonics*. Academic Press, London, pp. 173–191.
- Wendler, J.E., Wendler, I., 2016. What drove sea-level fluctuations during the mid-Cretaceous greenhouse climate? *Palaeogeogr. Palaeoclimatol. Palaeoecol.* 441, 412–419.
- Wendler, J.E., Wendler, I., Vogt, C., Kuss, J., 2016. Link between cyclic eustatic sea-level change and continental weathering: Evidence for aquifer-eustasy in the Cretaceous. *Palaeogeogr. Palaeoclimatol. Palaeoecol.* 441, 430–437.
- Wilmsen, M., Fürsich, F.T., Majidifard, M.R., 2015. An overview of the Cretaceous stratigraphy and facies development of the Yazd Block, western Central Iran. *J. Asian Earth Sci.* 102, 73–91.
- Yao, S., Gomez-Rivas, E., Martín-Martín, J.D., Gómez-Gras, D., Travé, A., Griera, A., Howell, J.A., 2020. Fault-controlled dolostone geometries in a transgressive–regressive sequence stratigraphic framework. *Sedimentology*. <https://doi.org/10.1111/sed.12739>.
- Yilmaz, I.O., Altiner, D., 2006. Cyclic palaeokarst surfaces in Aptian peritidal carbonate successions (Taurides, southwest Turkey): internal structure and response to mid-Aptian sea-level fall. *Cretac. Res.* 27, 814–827.
- Yose, L.A., Ruf, A.S., Strohmenger, C.J., Schuelke, J.S., Gombos, A., Al-Hosani, I., Al-Maskary, S., Bloch, G., Al-Mehairi, Y., Johnson, I.G., 2006. Three-dimensional characterization of a heterogeneous carbonate reservoir, Lower Cretaceous, Abu Dhabi (United Arab Emirates). In: Harris, P.M., Weber, L.J. (Eds.), *Giant hydrocarbon reservoirs of the world: From rocks to reservoir characterization and modeling*, AAPG Memoir 88/SEPM, Special Publication, pp. 173–212.
- Yose, L.A., Strohmenger, C.J., Al-Hosani, I., Bloch, G., Al-Mehairi, Y., 2010. Sequence-stratigraphic evolution of an Aptian carbonate platform (Shu'aiba Formation), eastern Arabian Plate, onshore Abu Dhabi, United Arab Emirates. In: van Buchem, F.S.P., Al-Husseini, M.I., Maurer, F., Droste, H.J. (Eds.), *Barremian – Aptian Stratigraphy and Hydrocarbon Habitat of the Eastern Arabian Plate*, 2. *GeoArabia Special Publication 4*, Gulf PetroLink, Bahrain, pp. 309–340.
- Zaitlin, B.A., Dalrymple, R.W., Boyd, R., 1994. The stratigraphic organisation of incised-valley systems associated with relative sea-level change. In: Dalrymple, R.W., Boyd, R.J., Zaitlin, B.A. (Eds.), *Incised Valley Systems: Origin and Sedimentary Sequences*, vol. 51. *SEPM Special Publication*, pp. 45–60.
- Zaitlin, B.A., Warren, M.J., Potocki, D., Rosenthal, L., Boyd, R., 2002. Depositional styles in a low accommodation foreland basin setting: an example from the Basal Quartz (Lower Cretaceous), southern Alberta. *Bull. Can. Petrol. Geol.* 50, 31–72.
- Zhang, H., Lü, F., Mischke, S., Fan, M., Zhang, F., Liu, C., 2017. Halite fluid inclusions and the late Aptian sea surface temperatures of the Congo Basin, northern South Atlantic Ocean. *Cretac. Res.* 71, 85–95.
- Zorina, S.O., 2014. Eustatic, tectonic, and climatic signatures in the Lower Cretaceous siliciclastic succession on the Eastern Russian Platform. *Palaeogeogr. Palaeoclimatol. Palaeoecol.* 412, 91–98.
- Zorina, S.O., 2016. Sea-level and climatic controls on Aptian depositional environments of the Eastern Russian Platform. *Palaeogeogr. Palaeoclimatol. Palaeoecol.* 441, 599–609.
- Zorina, S.O., Ruban, D.A., 2012. Hauterivian-Aptian (Early Cretaceous) transgression-regression cycles on the eastern Russian Platform and their inter-regional correlation. *GeoActa* 11, 41–50.